

AD-A174 864

APPLICATIONS OF FOCUSED ION BEAMS IN MICROELECTRONICS
(U) ROYAL SIGNALS AND RADAR ESTABLISHMENT MALVERNWOODEN
(ENGLAND) C BROUGHTON ET AL. APR 86 RSRE-MEMO-394886
DRIC-BR-100130

1/1

UNCLASSIFIED

F/G 28/12

NL



END
DATE
PAGE
NO.



MICROCOPY RESOLUTION TEST CHART
NATIONAL BUREAU OF STANDARDS-1963-A

AD-A174 864

UNLIMITED

ROYAL SIGNALS AND RADAR ESTABLISHMENT

Memorandum 3948

TITLE: APPLICATIONS OF FOCUSED ION BEAMS IN MICROELECTRONICS

AUTHORS: C. Broughton, M.I.J. Beale and V.G.I. Deshmukh

DATE: April 1986

SUMMARY

We present the conclusions of the RSRE programme on the application of focused ion beams in microelectronics and review the literature published in this field. We discuss the design and performance of focused beam implanters and the viability of their application to semiconductor device fabrication. Applications in the areas of lithography, direct implantation and micromachining and discussed in detail. Comparisons are made between the use of focused ion beams and existing techniques for these fabrication processes with a strong emphasis placed on the relative throughputs. We present results on a novel spot size measurement technique and the effect of beam heating on resist. We also present the results of studies into implantation passivation of resist to oxygen plasma attack as basis for a dry development lithography scheme. A novel lithography system employing flood electron exposure from a photocathode which is patterned by a focused ion beam which can also be used to repair mask defects.

Accession For	
NTIS GRA&I	<input checked="" type="checkbox"/>
DTIC TAB	<input type="checkbox"/>
Unannounced	<input type="checkbox"/>
Justification	
By	
Distribution/	
Availability Codes	
Dist	Avail and/or Special
A-1	



Copyright
C
Controller HMSO London
1986

UNLIMITED

RSRE MEMORANDUM NO 3948

APPLICATIONS OF FOCUSED ION BEAMS IN MICROELECTRONICS

C. Broughton, M.I.J. Beale and V.G.I. Deshmukh

CONTENTS

- 1 Introduction
- 2 Focused Ion Beam System Performance
 - 2.1 The RSRE/VG IBL100 focused ion beam implanter
- 3 Spot Size Measurement
- 4 Ion Beam Lithography
 - 4.1 Resolution
 - 4.2 Throughput Considerations
 - 4.3 Beam heating effects
 - 4.4 Alignment strategies
 - 4.5 Resist strategies
 - 4.6 Dry development ion beam lithography
 - 4.7 A novel lithography system
- 5 Direct Implantation Doping
- 6 Mask Fabrication and Repair of Masks and Devices
- 7 Micromachining, Amorphisation and Ion Beam Mixing
- 8 Conclusions

References

ILLUSTRATIONS - Figures 1-21

UNLIMITED

1 INTRODUCTION

Increasing attention is being paid to focused ion beams and their applications in microelectronic fabrication. Ion beams provide a flux of both material and energy which makes them suitable for many applications. Their use in direct write lithography potentially offers greater resolution and greater resist sensitivity than do electron beams. Direct doping, without the need for resist deposition, exposure, development and stripping, offers a much simpler processing schedule with potential for rapid device prototyping. The sputtering capability of finely focused high energy ions allows direct micromachining of materials and provides a high resolution secondary ion mass spectroscopy (SIMS) capability. Micromachining for optical mask repair has also reached the commercial marketplace and there is currently strong interest in the repair of X-ray masks and of integrated circuits.

The capabilities of focused ion beams have previously been reported in a number of reviews.¹⁻⁶ In this memorandum we examine each potential area of application in detail and compare the use of focused ion beams with the existing technologies to determine whether the potential advantages can be realised in practice. In particular, we make a detailed comparison of direct-write lithography with an ion beam and with an electron beam. An attempt is made to distinguish between the fundamental physical limitations of ion and electron beam systems and the limitations imposed by the current state of the technology that may be overcome as a result of further development. Reference is frequently made to the literature on focused ion beams and we highlight areas where further experimental work is required. We discuss the use of focused ion beams in the following sections; system performance, lithography, direct doping, mask fabrication and repair, micromachining, amorphisation and ion beam mixing. The application of ion beams in each of these possible areas is compared with existing process techniques for production scale fabrication of integrated circuits with emphasis being placed on the low throughput of focused ion beams. We do not consider materials analysis applications in which the use of focused ion beams is well established.

We discuss general design considerations and performance capabilities of focused ion beam implanters and make specific reference to the focused ion beam machine at RSRE; a VG Semicon IBL100. Particular emphasis is placed on the comparison between electron and ion beams for direct-write lithography as this was originally the main motivation for the development of the IBL 100. The effect of each of the main parameters on wafer throughput is analysed in detail. We outline the specifications of the VG IBL 100 and discuss the short-comings of the equipment.

We present experimental results obtained during the programme including the techniques developed for the measurement of the sub-micron spot size and the effects of beam heating on the resist. Our work on the elucidation of the mechanism by which ion implantation results in passivation against oxygen plasma attack is also outlined and the application of this effect to provide an all dry development ion beam lithography is discussed.

The requirements of the ideal lithography system are discussed and a novel flood electron beam exposure lithography system which meets these criteria is described. The system employs a focused ion beam for both the patterning and repair of the photocathode mask.

The programme started with the arrival of a VG IBL100 focused beam implanter in late 1984 and continued for 18 months. The work was terminated due to problems with the equipment and to the lack of promise shown by the technique. We conclude that focused ion beams are not a viable approach for either lithography or for direct doping for standard device fabrication. However, they may have applications in mask repair, for a number of special, hand-crafted devices, for materials and devices research purposes and, possibly, for the novel lithography system proposed.

2 FOCUSED ION BEAM SYSTEM PERFORMANCE

Submicron focused ion beams have been formed using electrostatic optics and either liquid metal ion sources (LMIS)⁷⁻¹⁵ or liquid hydrogen or helium field ion sources.^{16,17} Other types of ion source do not have sufficient brightness to allow the formation of submicron beams with useful current densities.¹⁸ LMIS have been the subject of much study over recent years and, due to their ease of construction and operation, are used almost exclusively in focused ion beam equipment. The availability of ion species from LMIS is restricted since the source metal is required to have a reasonably low melting point, a vapour pressure compatible with vacuum operation, the ability to wet the support needle and to be relatively inert in reaction with the needle. However, due to appropriate alloying of metals, a useful range of species has become accessible.⁴ Although LMIS brightness is equivalent to a LaB₆ electron source ($10^6 \text{ A cm}^{-2} \text{ sterad}^{-1}$) their total particle flux is much less and large currents cannot therefore be extracted. As the extract current is increased to greater than about 30 μA , the emission becomes unstable and droplets of the source metal are given off.¹⁹ For sources other than gallium and indium, operating lifetimes may be only a few hours.

The dominant factor limiting resolution with columns using LMIS is chromatic aberration^{3,4,20} as the energy spread of the ions is relatively high and increases with the extracted current.^{4,19} The chromatic angular intensity of a gallium source achieves a minimum when the extract current is approximately 2 μA ,²¹ this is therefore the normally chosen operating current. This extraction current is three orders of magnitude lower than that obtained from electron sources.²²

Beam current densities produced by ion columns are typically 1 A cm^{-2} ,⁴ a factor of approximately 200 less than that can be achieved with electron beam columns.^{22,23} This is due to both the higher currents obtainable from electron sources and to the better optical performance of electron columns. Ion column design is receiving attention and Wagner⁴ believes that "there is reason to be optimistic that large increases in current density can be achieved". Indeed Kurihara²⁴ has recently reported a column design theoretically capable of producing a current density of 40 A cm^{-2} using a Gallium LMIS. Despite these advances however, it does not seem likely that ion optics with LMIS can be improved to equal the performance of electron optics and sources.

The higher source brightness and lower energy spread of the gas field ion sources²⁵ should provide current densities of approximately 100 A cm^{-2} , i.e. comparable with electron sources. Siegel et al.²⁶ have designed a focusing column for the hydrogen field ion source which is theoretically capable of providing 260 A cm^{-2} into a 100 \AA spot or 160 A cm^{-2} into a 500 \AA spot. However, Blackwell et al.¹⁶ and Itakura et al.¹⁷ have reported that these

sources are difficult to operate and are far from achieving in practice the theoretically predicted performance.

Orloff and Sudraud²⁷ have designed a high resolution column utilising a LMIS and employing Koehler illumination to overcome the problem of source size. With this approach, a 1 μm aperture is demagnified 100 times to produce a final probe size of 100 \AA . The concomitant penalty is that the beam current is reduced to only approximately 1 pA.

In ion optical column design, consideration must also be given to beam deflection and blanking. The greater mass-to-charge ratio of ions than electrons produces a much stiffer beam which, for a given deflection system capability, results in smaller exposure fields. The "time of flight" of ions is also an important factor; a 20 keV electron has a velocity of $8 \times 10^7 \text{ m s}^{-1}$ whereas for a 100 keV proton the velocity is $2 \times 10^5 \text{ m s}^{-1}$. In consequence, the transit time of the ions in the optical components is relatively long and becomes comparable to the time available for deflection and blanking when operating at high scan frequencies. The design and operation of a system operating in this regime becomes very complicated.

A further problem in the design of ion beam columns is that beam limiting apertures are prone to extremely high implantation doses and will therefore have very short lifetimes. In consequence, some of the techniques used to increase throughput in electron beam machines, such as shaped beam and multi-beam systems,²² may not be directly transferable to ion beams.

2.1 The VG/RSRE IBL100 focused ion beam implanter

The performance of the VG IBL 100 is now outlined. A schematic diagram of the ion optical column is shown in figure 1. The column consists of an ion gun (a), based on a liquid metal ion source, and two electrostatic lenses (c,f) which focus the beam onto the sample which rests on an X-Y and rotatable stage (h). Adjustable beam limiting apertures (b) are situated above the first lens to restrict the beam current and beam blanking plates (d) are at the image plane of the first lens to provide conjugate blanking. A quadrupole stigmator (e) is provided just below the beam blanking plates and the beam steering plates (g) reside below the final lens. A scintillator (j) acts as a secondary electron detector to allow imaging. The system includes a removable Wien velocity filter, for separation of ions from a multi-element source, which is inserted just below the ion gun and above the adjustable apertures. The equipment operates at ultra high vacuum (UHV), typically 10^{-10} torr, and has a specimen loading and preparation chamber with a transport system (through channel k) into the exposure chamber. Sample handling is exclusively for wafers of 3 inches in diameter.

The pattern generation hardware and software was designed, developed and built at RSRE and is based on the system developed for the electron beam lithography equipment. A schematic diagram of the computer controlled pattern generation system is shown in figure 2.

The system was specified for operation from 20 to 100 keV, with a beam current in excess of 0.1 nA and a spot size of 500 \AA at 50 keV. The system performance fell short of the specification in a number of areas. Operation at or near 100 keV was unreliable due to breakdown of the electrostatic lenses and leakage across the gun isolating insulator. This resulted in the

generation of X-rays and the excessive currents drawn destabilised the EHT power supply. Despite conditioning the column, by maintaining the maximum voltage (100 keV) on the HT elements with a relatively high current supply to produce field accumulation at any "sharp" points leading to subsequent breakdown knocking off such points, high voltage operation remained unreliable. Low voltage operation (less than 40 keV) proved difficult as the beam current was reduced to such an extent that observation and focusing of the image became difficult.

Source operation was also problematic. The gallium source failed several of times due to contamination. Analysis revealed that the source was initially heavily contaminated with copper. This was found to be due to the gallium loading procedure employed by the supplier and was then rectified. The gallium source often proved difficult to start, especially after baking the system to $^{\circ}150$ C to achieve UHV conditions. Close examination of the source after baking revealed a skin like structure covering the needle. If the system was not baked, the source operation became more stable and reliable. The vacuum in the vicinity of the source may have contributed to the source operating problems; the top of the column was poorly pumped through narrow ports and although no vacuum guage was present to monitor source operating pressure, a very poor vacuum was suspected in this critical region. The poor pumping would be particularly worrying when operating the high temperature silicon-gold source. However, due to mechanical incompatibility the silicon-gold source could not be fitted at first. Following rectification, ion emission from the source was not achieved and no further tests were performed due to termination of the programme. Problems were also incurred with the mass filter; installation was clumsy and unsatisfactory and it proved impossible to align this unit with respect to the rest of the column. Therefore the filter could not be tested.

The spot size failed to meet the 500 Å specification and was approximately 1500 Å at best. The measurement method is described below. Factors thought to contribute to the relatively large spot size include; poor EHT stability, high susceptibility to acoustic pickup due, primarily, to the cantilevered lens supports, problems in alignment of the column and the very large working distance (10 cm). A complete redesign of the equipment would be necessary to meet the 500 Å specification.

Beam deflection and blanking was also problematic. No beam blanking was supplied until after the termination of the programme. Reliability was a tremendous problem, downtime exceeded 90% over the year of operation. Repair was hampered by lack of accurate documentation and lack of technical support from VG.

3 SPOT SIZE MEASUREMENT

Measurement of the spot size of a focused electron beam is conventionally performed by scanning over a sharp edge located over a Faraday cup. The spot size is determined from the current collected by the cup as the beam is scanned over it and the width is typically taken as the distance scanned between 10% and 90% of the maximum collected current. With an ion beam, this method is less straightforward due to the sputter erosion of the sharp edge by the focused beam. Furthermore, the high yield of secondary ions and electrons further complicates the measurement. We have developed a novel technique to measure spot size; this uses a crystalline silicon target

which is implanted in a series of stripes. These stripes are scanned at a fixed beam current but with a range of different scan speeds to give a series of different doses. Silicon is amorphised by ion doses in excess of approximately 10^{14} ions cm^{-2} for heavy ions such as gallium. The silicon substrate is then examined by cross-sectional transmission electron microscopy (TEM) to determine the width of the amorphised stripes.

Regions of amorphous silicon in a crystalline substrate are clearly visible under diffraction contrast conditions in TEM. Figure 3a shows a bright-field image of the cross-sections of five lines implanted on the IBL100 with 100 kV gallium at five different doses, the amorphous regions appear dark against a light background. Figure 3b is an enlargement of the widest stripe and demonstrates that the resolving power of this technique is less than 100 Å. To extract information about the beam profile from these data, the widths of the implanted stripes are plotted against their implant dose, as shown in figure 4. The data points can then be fitted to a curve, in this case a gaussian, that defines the beam profile. Note that using this approach it is not necessary to know the value of the amorphisation threshold, only to assume that it is a constant under the implant conditions used i.e. that the edge of the amorphous zone corresponds to a specific ion dose at that point. Of the three curves plotted in figure 4, curve b is the closest fit and yields a standard deviation of 875 Å. This value is equivalent to a 10% to 90% width of 1700 Å.

A further technique we have developed for spot size measurement is also based on the amorphisation of lines in silicon with different doses. The linewidth is however determined by scanning electron microscopy of the lines. Contrast is obtained by etching out the amorphised silicon by immersion of the sample in hydrofluoric acid. This technique is rapid and simple and early results are promising. However, we have not yet compared the results obtained with this method with those obtained by the TEM method to ensure that the etch removes all of the amorphised region cleanly from the crystalline material.

A quick in-situ method was also used to measure the beam spot size. The method is a variation on the standard method described earlier for electron beam spot size measurements in which the beam was scanned over a sharp wedge tapering to a very thin but well defined edge. The sample was fabricated by anisotropically etching single crystal silicon²⁸ and then sputter depositing a thin gold film to increase the secondary electron yield. The use of a sharp wedge has the advantage of reducing the normally enhanced ion induced secondary electron yield near the sample edge. This enhancement is due to the effect of the edge geometry and confuses the determination of the spot size. With the sharp wedge, the profile obtained falls monotonically as shown in figure 5, making analysis straightforward. Sputtering of the edge of the sample remains a potential problem but in practice good agreement has been obtained with the TEM measurement method, both giving a 10% to 90% width of 1700 Å.

4 ION BEAM LITHOGRAPHY

In comparison with electrons, the short range and high rate of energy deposition of ions in matter provides enhanced pattern resolution and resist sensitivity. To assess whether ion beams are a viable technology for lithography we compare their performance with electron beams.

4.1 Resolution

Lateral scattering of electrons as they penetrate the resist produces an effective broadening of the focused spot. In addition, backscattering of the electrons from the underlying substrate produces the so called proximity effect.²⁹ Ions are scattered over significantly shorter distances giving rise to reduced effective broadening of the focused spot and no proximity effect. In the case of electrons, high accelerating voltages have been employed to reduce greatly the effects of electron scattering. For example, 100 Å lines have been delineated on standard substrates³⁰ and features as small as 44 Å have been produced on thin membrane substrates.³¹

A fundamental resolution limitation of both ion and electron beam lithography is the scatter of the secondary electrons within the resist. It has been reported that the secondary electrons produced by ions are of lower energy than those produced by electrons.^{1,32} In the case of ion beams, a further potential resolution limit arises from recoil atom scattering.³³ Linewidths of approximately 300 Å have been produced with 30 keV protons using masked ion lithography.³³ However, in practice, the resolution of focused ion beams is presently equipment limited. It seems unlikely that ion beams will achieve the few angstroms diameter spot sizes that are routinely obtained with electrons.

4.2 Throughput considerations

Here we consider the major factors that contribute to the throughput of direct write lithography and compare the performance of electron and ion beams systems. Ion beams must provide significant throughput and resolution advantages in order to motivate the major research and development effort that would be required to displace the existing electron beam approach. We discuss in turn the factors which affect wafer throughput; resist sensitivity, usable beam current and pattern definition rate.

In order to illustrate the factors affecting throughput, figure 6 shows the exposure time per wafer level against resist sensitivity for two different beam current densities. These calculations assume 1% coverage of a 4 inch wafer (80 mm²) and a beam spot size of 0.25 microns. The two beam current densities were chosen as those typical of a focused ion beam (1 A cm⁻²) and a focused electron beam (100 A cm⁻²). The corresponding beam currents are 0.49 nA and 49 nA respectively. The area to the left of the vertical dashed line denotes the regime of resist sensitivities where the number of particles required to expose a pixel is so small that statistical fluctuations in the beam current becomes significant (see below). The area above the horizontal dashed line represents exposure times in excess of 8 hours and therefore, beyond sensible consideration. In the case of the 1 A cm⁻² exposure line, the transition from a solid line to a dashed line represents the maximum resist sensitivity reported.³⁴

Figure 7 illustrates the effect of spot size or equivalently, pixel dimensions on the exposure time. This exposure times assume a beam current density of 100 A cm⁻² and only 1% coverage of a 4 inch wafer.

Because ions have much shorter range in resist than electrons, the energy density deposited is higher and consequently the resist sensitivity is

greater. Reported sensitivity enhancement factors for different resists range from 7.8 to 270 for 100 keV protons³⁴ and even higher for more energetic and more massive particles.^{1,32,35-40} In general, resists with higher electron sensitivity show a lower enhancement factor when exposed to ions. The energy density in an individual interaction cascade may exceed that actually required for full resist exposure in that volume and the excess energy does not therefore contribute to the exposure.³¹ This reduced utilisation of the deposited energy would result in a lower enhancement factor than that expected from the average energy deposition. Conversely, some resists are more sensitive to ion irradiation than might be expected from electron exposure, this is thought to be due to exposure being effected by a two site activation mechanism.³² In practice, the range of available sensitivities is smaller for ion exposure. An important practical consequence of the enhanced sensitivity and its smaller range is that resists may be chosen for their process tolerance rather than for their sensitivity alone.

It is important to consider both the resolution and the sensitivity of a resist as there is generally a trade-off between the two. For a resist to have high sensitivity, the volume of resist modified by each incident particle must be relatively large as the mean distance between incident ions is large; hence, the resolution is low. Taking a binary exposure approximation in which a pixel is either exposed or unexposed, then the minimum number of particles, N , required to expose a pixel of dimension L is :-

$$N = S.L^2 \quad (1)$$

where S is the resist sensitivity (ions cm^{-2}). N must obviously exceed unity, setting an upper limit to the usable resist sensitivity. In reality statistical fluctuations in the beam current place an increased lower limit on N thereby further reducing the maximum usable resist sensitivity. Attempts have been made to define the minimum value for N that keeps statistical fluctuations to an acceptable level for device fabrication. Assuming a binary exposure model, Greeneich²⁹ proposes a lower limit of $N = 200$ (electrons per pixel) based on shot noise considerations. Macrander et al.⁴¹ used a negative resist exposure model and concluded that 3200 ions would be required to expose a resist of a contrast of 2 with a 10% linewidth error probability of less than 10^{-10} . They also showed, using a Monte-carlo technique, that a minimum of 1200 ions per pixel were required for uniform exposure of a $0.1 \mu\text{m}^2$ pixel.

Cleaver et al.⁴² suggested that noise was responsible for roughness of the channel floor and irregularities in the line edge of a gallium exposure of PMMA. The mean exposure dose used was 3×10^{12} ions cm^{-2} and they estimated the dose at the line edge to be 2×10^{12} ions cm^{-2} , which, according to Namba⁵ is sufficiently low to make statistical fluctuations significant.

It is not clear how one should compare these different studies as each approaches the problem from a different viewpoint and assesses the effects of noise differently. Experimental work is evidently required to clarify the situation. The number will be dependent on the ion species and energy, resist characteristics, pixel size and the required linewidth control. Statistical noise is likely to be a greater problem for ion exposure than for electron exposure because of the greater resist sensitivity. Figure 8 shows a plot of pixel size (spot size) against resist sensitivity in which

the three lower limits proposed by the authors cited above are shown as three lines. According to these authors, the regions below these lines are expected to result in unacceptable statistical fluctuations.

The rate at which individual pixels can be exposed is a basic limitation on the throughput of any direct write lithography system. For a given deflection capability, as the pixel size is reduced so their number increases as a square law and the throughput is therefore reduced as a square law. Consequently, direct write lithography throughput falls very rapidly as feature sizes are reduced. With a conventional gaussian beam, the maximum exposure rate is limited by the deflection electronics. Attempts to overcome this problem essentially involve parallelism in the exposure strategy. Electron beam machines have been developed which use multiple beams or variable shaped beams to provide effective pixel exposure rates of 750 MHz and 2.5 GHz respectively¹⁹, far beyond the capability of vector scanned systems. However, the value of these approaches to ion beam lithography will be much reduced due to the relatively low source current available.

Wafer throughput will be reduced by machine overheads including wafer handling, vacuum pumping, stage movement, alignment and optimisation of the optics. The limitations with ion beams will be similar to those with electron beams and will not be considered in detail.

4.3 Beam heating effects

Throughput limitations imposed by beam current considerations are now discussed. As previously discussed, the beam current available at the sample is determined by the properties of the source and the focusing optics. However, the maximum current density that can be used may be further limited by sample heating effects. The temperature rise in the implanted region of the sample is determined by the current density, accelerating voltage, dwell time, spot size and the thermal conductivity of the sample. We are here considering the equilibrium temperature in the region near to each implant cascade and not the non-equilibrium "thermal spike" effects that may occur on relatively short timescales.

Temperature effects arise both for electron and ion irradiation and are utilised for example in electron beam welding. Brown and Wagner⁴ discussed heating effects during direct implantation into silicon and showed that they are not significant for the available current densities and spot sizes. However, our calculations and experimental results show that heating effects are much greater for resist implantation due to its much lower thermal conductivity and can be very significant. Temperature effects include the formation of blisters and other surface features and the modification of exposure and development characteristics. The value of any future major improvements in ion sources and optics may well be restricted by these thermal effects.

Blistering and the formation of other topographical features can occur when high dose rates are employed. During our exposures with the IBL100 we have noticed the effects of beam heating on polymethylmethacrylate (PMMA), some of which are shown in Figure 9. Quite different features occur reproducibly at different doses and dose rates. We have not yet elucidated the mechanisms of their formation.

The time taken to heat the resist to its glass transition temperature (assumed to be 200 °C) as a function of average beam current density is displayed in figure 10. This is not necessarily the critical temperature for these effects but is arbitrarily chosen as a reference temperature. These calculations assume a uniform hemispherical heating model⁴³ with a beam radius of 875 Å and ion energy of 80 keV. To avoid heating the resist to 200 °C the dwell time must be kept to less than that indicated by the curve. This phenomenon has consequences upon the throughput of a direct lithography system as it may not be possible to use higher current densities to achieve higher throughput.

4.4 Alignment strategies

An important requirement of any lithography system is fast and accurate layer to layer pattern alignment. Successful alignment requires that the markers can be both easily recognised and resolved to the required accuracy. In electron beam lithography, electrons backscattering from the substrate can re-emerge from the resist due to their relatively large range thereby providing a mechanism for imaging buried alignment markers.⁴⁴ In the case of ion beam lithography however, the ions have very limited depth of penetration and cannot provide information about alignment features below the resist layer. In any case, the ion range would generally be restricted to avoid substrate damage. Consequently, it is impossible to image alignment markers beneath the resist. A satisfactory solution to layer-to-layer alignment with ion beam lithography has yet to be proposed and remains a major hurdle to establishing the credibility of ion beam lithography even for specialised low throughput applications.

4.5 Resist strategies

The ion sensitive layer in a resist structure must be exposed to its full depth prior to development. In general, the ions must be prevented from reaching the underlying substrate or the resultant damage will have a severely deleterious effect on device performance. Only under a very restricted range of conditions can subsequent annealing be expected to remove the ion bombardment damage. In consequence, a bi-level or tri-level resist system, consisting of a thin ion sensitive resist on top of a thick ion absorbing layer, must be used. The thickness of the absorber layer must be sufficient to stop effectively all ions from reaching the substrate. For example, consider the exposure of 0.4 µm of resist with 200 keV silicon ions, their peak projected range and standard distributions are 0.44 µm and 0.1 µm respectively. To prevent all substrate damage (say 10 standard deviations) would require a total layer thickness of approximately 1.5 µm.

4.6 Dry development ion beam lithography

Ion implantation of PMMA is known to modify its etch rate in an oxygen plasma. This effect can be used as the basis for a lithography system based on ion beam exposure and dry development.⁴⁵ We have systematically investigated the role of the main implant parameters, species, dose and energy, in order to elucidate the mechanisms involved and thereby optimise to implant and development conditions. The ability to develop a patterned resist by plasma processing is attractive and would be consistent with the general trend towards all dry processing. A major disadvantage of this

approach is that reported resist sensitivities are several orders of magnitude lower than for the wet development of organic resists exposed by either ions or electrons.⁴⁶

We investigated the ion beam passivation of polymethyl methacrylate (PMMA) to attack by oxygen reactive ion etching. Previous work has reported resist passivation to dry etching after gallium,^{45,47} indium⁴⁸ and silicon ion implantation.⁴⁹ These authors suggested that the passivation effect was achieved by the formation of an etch resistant surface film which was formed by the oxidation of the implanted species during the dry etching stage. Unconvinced by this explanation we showed that the passivation effect was also produced by the inert ion argon showing that the mechanism for passivation was not well understood. We have re-examined the the passivation process to try to determine the role of the main implant parameters and have investigated the change in the resist composition after implantation.

Ga⁺, Ar⁺, B⁺, and H⁺ ions were implanted with energies between 35 and 180 keV and doses between 10¹⁴ and 10¹⁶ ions cm⁻² using a Lintott Series 2 implanter. Some samples were also "implanted" with electrons in a Cambridge Instruments EBMF 2 electron beam lithography system. A dose of 5x10¹⁶ ions cm⁻² was implanted at 20 keV. Dry development was performed in a Plasma Technology 80 etcher with 2 mtorr oxygen pressure, 3 sccm flow rate and 20 Watt power input (equivalent to 88 mW cm⁻²). A reactive ion etching (RIE) mode was used to maximise the anisotropy of the etching process.

In all cases, implantation caused a reduction of the PMMA film thickness which exceeded 0.5 μm for some of the implants investigated. The loss increases with implant dose before saturating above a critical dose and also increases with implant energy. This thickness loss is caused by the resist losing material due to outgassing during exposure. The species evolved during implantation were identified by using residual gas analysis with a quadrupole mass spectrometer. Figure 11a is the residual gas mass spectrum of the atmosphere in the IBL100 and is typical of a UHV system. Figure 11b is the mass spectrum obtained while exposing PMMA to 80 keV Ga⁺ ions. We notice a significant rise in the abundance of masses 12, 13, 14, 15, 16 and 28 indicating that methane and carbon monoxide are being evolved during the exposure process.

To study the characteristics of the outgassing more closely, the partial pressure of mass 16 was recorded as a function of dose for two different dose rates. Figure 12 depicts the dependence of the partial pressure of mass 16 on dose at a rate of approximately 2.7x10¹³ ions cm⁻² s⁻¹ and figure 13 shows the same for a dose rate of approximately 4x10¹² ions cm⁻² s⁻¹. The curve of figure 12 shows saturation at approximately 10¹⁵ ions cm⁻² which is the same dose for saturation of thickness loss, as should be expected. However, the inflexion in the curve prior to this is not understood.

Figure 14 shows the resist thickness removed by the plasma etching process as a function of etch time for unimplanted PMMA and for PMMA which had been implanted with 40 keV Ga⁺ ions. Figure 15 shows similar curves for PMMA implanted with 180 keV Ga⁺ ions. We observed that implantation reduces the etch rate in the near surface region of the resist while at greater depths the etch rate remains unaffected. Within the implant-modified region of

the resist, the etch rate is dependent on ion dose and range. Although the etch rate decreases with increasing ion dose, the dependence is non-linear and saturates at approximately the same dose as does the thickness loss. The depth of the implant-modified resist increases with increasing ion range.

The etch rates were measured on samples implanted with other species, viz. argon ions (65 keV, 10^{15} cm⁻²), boron ions (40 keV, 10^{16} cm⁻²), hydrogen ions (100 keV, 10^{15} cm⁻²) and electrons (20 keV, 5×10^{16} cm⁻²). The dry etch behaviour follows the same trend as with the gallium implanted samples and is displayed in figure 16. Resist passivation occurs with each of these implanted species.

SIMS, with a caesium ion beam, was used to examine samples implanted with 10^{16} cm⁻², 40 keV boron ions. The relative concentrations of the oxygen, carbon and hydrogen were broadly similar in the unimplanted and implanted films. The oxygen concentration in both unimplanted and implanted films was confirmed using the nuclear reaction $O(D,\alpha)N$. The transmission infra-red (IR) absorption spectra from the unimplanted PMMA showed characteristic peaks associated with carbonyl bonds (figure 17). After high dose implantation the absorption peaks present in the unimplanted film were absent and a relatively featureless spectrum was obtained (figure 18).

Our results show that ion implantation modifies the resist in three ways; that is a reduction in resist thickness, a reduction in the dry etch rate and changes in the carbon bonding. For a given implant species, these effects all become significant at approximately the same dose. Furthermore all three effects saturate at approximately the same dose.

As all the species studied result in these effects, we suggest that they are due to the energy deposited by the implant and not to the implanted species itself. We now relate the energy deposited by each implant species to its effect on the resist properties. The combined electronic and nuclear losses per unit projected distance is approximately constant for the majority of the ion range, falling rapidly near the end of the range. The constant value of the dry etch rate in the ion modified region of the resist and its abrupt change to the rate characteristic of the unmodified resist is entirely consistent with these energy deposition profiles.

If we arbitrarily define a critical implant dose which results in an etch rate reduction of a factor of two, then this dose will depend upon the nature of the incident particle. However, if we calculate the energy density deposited by the critical dose of any particle then we find that this is a constant and is independent of the nature of the implanted species. Its value is approximately 10^{24} eV cm⁻³, equivalent to between 10 and 15 eV per atom in the original film.

Our results suggest that the resist passivation effect occurs for any implanted species, including electrons, and that the passivation is a consequence of the energy deposited in the resist. There is no evidence for chemical or other species dependent effects in the passivation process. As the effect of implantation is simply to deposit energy into the polymer, the optimisation of the implantation parameters simply involves choosing the ion species and energy to deposit a maximum of energy into the required thickness of resist. Results of IR absorption, SIMS and nuclear reaction analysis show the implantation results in the destruction of the original

chemical bonds present in the film and in the formation of a heavily modified structure containing high concentrations of carbon, oxygen and hydrogen.

The motivation for studying this phenomenon was to produce a dry developable resist process using focused ion beams. Figure 19 contains micrographs of features drawn with the IBL100 and subsequently etched as described above. The exposure dose chosen was 5×10^{15} ions cm^{-2} as this was within the saturation region of the passivation effect. The ions used were 50 keV Ga^+ except for figure 19b for which 60 keV Ga^+ ions were employed. All the features resolved suffered from surface roughness or holes which we can attribute to beam heating of the resist.

This dry development lithography scheme may have specific applications but suffers from all the problems associated with ion beam lithography that were discussed previously. The throughput problem is exacerbated by the much higher doses needed to achieve the dry etch passivation effect. However, these results may be relevant to plasma etching of organic resists as this process involves the low energy implantation of both ions and electrons at very high fluxes. In particular, we suggest that electron beam irradiation may be used for resist hardening prior to plasma etching.

4.7 A novel lithography system

Consideration of a lithography system suitable for high throughput sub-micron semiconductor device fabrication suggests the following points;

- a) Exposure must be performed in parallel by flood beam; necessary to achieve high throughput.
- b) Exposure with charged particles is preferable; beam manipulation, focusing, distortion correction and alignment are simpler.
- c) The charged particles should be emitted from the mask rather than transmitted through it; this eases the design constraints on the mask and the chromatic aberrations due to large energy spread.
- d) The charged particles causing the exposure should be electrons rather than ions; electrons are more easily generated and manipulated and will not damage the mask during exposure.
- e) Mask formation must be a serially written process and should be performed by ions; the mask must be insensitive to the electrons generated during the exposure process.
- f) Mask fabrication, inspection and repair should be performed in the same piece of equipment. Wafer exposure could also be performed in the same equipment.
- g) Proximity effects should be minimal suggesting the use of 50 to 100 keV electrons; software correction is messy.

We suggest the following novel system which meets these criteria.

A focused ion beam is used to pattern a photocathode mask. This is then illuminated by a flood beam of photons and the photoelectrons emitted

expose the resist. The system combines mask fabrication, inspection and correction with resist exposure.

In this system, the resist exposure is performed by electrons emitted from the surface of the mask. The electrons are photo-electrons generated by flood exposure of the mask with photons of appropriate energy. The photo-electrons are focused and accelerated onto the target wafer using magnetic and/or electric fields. The electrons should be accelerated by 50 to 100 keV in order to overcome proximity effects in the resist.

The mask is a photocathode whose surface properties have been modified by ion implantation using a scanned focused ion beam. The aim of the implant is to modify the quantum efficiency of the photo-electric yield. A key point is that the photocathode material is chosen so that the implantation induced modifications are reversible. The ability to reverse and re-write the modifications allows mask repair and design modifications to be performed easily.

The use of a photo-cathode is not novel. A 0.25 μm resolution, 20 keV system has been developed at Phillips using a CsI photo-cathode. This system is purely a resist exposure system and does not involve mask fabrication, inspection and repair as in the system we propose. The key advantages of our system is the use of a repairable mask, with mask checking and repair being performed in the same piece of equipment as the exposure.

A possible implementation of this concept is now suggested. A crystalline silicon photocathode is implanted with a focused ion beam so that certain areas are amorphised in the pattern required for the exposure. The photo-electric quantum efficiency of the amorphised regions will be lower than that of the unimplanted regions. The quantum efficiency is highly sensitive to the surface condition, but as yet we have not quantified the effect of amorphisation.

The resist exposure is performed by flood illuminating the photocathode with 6 eV photons and accelerating the emitted photo-electrons onto the target resist. An accelerating potential of 75 keV would eliminate proximity effects. Magnetic and/or electric fields are used to focus the photo-electrons from the photocathode onto the resist. The projection optics could be 1:1 or may demagnify the photo-cathode in order to reduce resolution requirements during mask making and to increase the current density for the exposure. It may be necessary to shield the resist from illumination by the flood photon beam, this could be achieved by a thin metal layer deposited on the resist.

After implantation of the photocathode, a scanned electron beam can be used to check for defects. Either the photocathode itself can be scanned or a suitable test target that has been exposed. If a "clear" defect is found then the crystalline silicon can be re-implanted and if an "opaque" defect is found then it may be locally heated to 600 °C with a higher power electron beam to epitaxially regrow the amorphous material to crystalline silicon. The repairability of the mask is a key feature of this system.

In principle, a single piece of equipment could be built with ion beam mask fabrication, mask checking using a scanning electron beam, mask repair using a high power electron beam and finally resist exposure using imaged

photoelectrons generated by flood photon exposure of the photocathode.

Many variations on this basic concept are possible. Photoelectrons are particularly suitable for the resist exposure as their low energy spread makes high resolution focusing relatively easy. Secondary electrons or backscattered electrons with their higher energies and energy spreads would make focusing difficult. The electrons could be emitted by flood optical or UV irradiation of the mask. The source of the illumination could be either behind or in front of the mask depending on the properties of the photocathode. Design would be simplified if back illumination could be employed, for example a silicon on sapphire wafer might be used to give a single crystal silicon layer with an optically transparent rigid backing layer.

The photon energy would be determined by the photocathode used, in the case of silicon, germanium or gallium arsenide photon energies of approximately 6 eV (200 nm) are required and give a yield of approximately 10^{-3} electrons per photon. At 5 eV the yield has fallen orders of magnitude. Other materials such as CdTe, CdS, caesiated Si, caesiated GaAs and caesiated GaP have quantum efficiencies two to three orders of magnitude higher (approximately 1 electron per photon) but it is not obvious how defects in these photocathodes could be repaired and furthermore their preparation and treatment is non-trivial. Silicon is the only material that readily regrows epitaxially perfectly after ion amorphisation. Germanium is also probably good but has a less stable surface oxide. GaAs and GaP regrow to some extent.

To expose a resist with a 1:1 projection system with 10^{13} electrons cm^{-2} with 6eV photons an incident light flux of 10 mW cm^{-2} results in a 1 second exposure. This assumes a quantum efficiency of 10^{-3} , appropriate for very clean (UHV) silicon, a native oxide absorbs 94% of the photoelectrons. If the quantum efficiency of a practical system was 10^{-5} rather than 10^{-3} then the light flux for a 1 second exposure is 1 Watt.

The difference in quantum efficiency of silicon is also affected by doping. Degenerately doped p-type has a factor ten higher efficiency than degenerately doped n-type at 5.5 eV and the yields are approximately the same at 6.5 eV. The difference in quantum efficiency could be maximised, at the expense of total yield, by selecting the doping level of the silicon and the energy of the illumination.

An alternative approach to the use of ion amorphised silicon is the use of a caesium liquid metal ion source to direct-write a high quantum efficiency photoemitter onto a low efficiency substrate. The implant may be to caesiate the surface of, for example, silicon or gallium arsenide or it may be to form a stable high efficiency compound such as CsI, as used in the Phillips system. The problem with this approach is that a repairable system is less easy to envisage. Ion milling using a gallium source for example could be used to remove "clear" defects while "opaque" defect could be written over using the caesium source. The sensitivity of the surface to contamination suggests that compound formation is the best route.

The silicon photocathode system appears promising and is the simplest implementation of the concept. The literature suggest that crystalline silicon has an adequate quantum efficiency under 6eV illumination provided the surface is atomically clean. We need to assess the efficiency under the

conditions of interest (HV not UHV) and to see the effect of amorphisation. Existing knowledge suggests that the quality of regrown amorphous layers of silicon will be adequate. The lifespan and resolution of the patterned photocathode must be assessed. Phillips have already demonstrated that a patterned photocathode (CsI) can be imaged onto a wafer and used for high throughput submicron lithography. Thus it appears that the most difficult part of the development is already proven.

5 DIRECT IMPLANTATION

Probably the most elegant and appealing application of focused ion beams is device fabrication by direct dopant implantation without the need for any lithography steps. This offers great process simplification, the possibility of laterally varying dopant concentrations and the ability to prototype devices rapidly. Work to date^{42,50-55} has shown that the electrical characteristics of implants performed with a focused beam are broadly similar to those done conventionally. An exception being the implantation of light ions such as boron, where the high dose rates employed with focused ion beams amorphise the implanted silicon and thereby allow dopant activation after annealing at relatively low temperatures.^{56,57}

We now highlight some of the factors which must be considered if the potential of direct doping is to be realised. There is only a limited range of species currently available with liquid metal ion sources as already discussed. Direct write implantation falls foul of the same throughput constraints as direct write lithography. The situation is even worse as typical implantation doses for standard device fabrication range upto 10^{16} cm⁻², orders of magnitude greater than those required for resist exposure, with a corresponding decrease in throughput. Conventional implantation can not therefore be replaced by direct implantation for standard integrated circuit fabrication. However, it may be appropriate for specific applications and for special, high value devices.

Using a scanned focused ion beam, laterally varying doping profiles can be achieved more simply than by other techniques. Reuss et al.⁵⁴ have shown that current crowding in a bipolar npn transistor can be reduced by tailoring the doping profile to produce improved device performance. However, to implant even 1% of a 4 inch wafer with the dose range reported, 8×10^{12} to 8×10^{13} ions cm⁻², with a beam current of 0.1 nA would take 2.5 hours to 25 hours without allowing for any other throughput limitations.

A serious limitation to direct doping arises from the frequent device requirement for very high dopant concentration gradients. The lateral distribution of the implanted ions is determined by the gaussian beam profile, lateral ion scattering and diffusion during annealing. In illustrating the problem, we shall assume the latter effects are relatively insignificant and they are ignored, ie the lateral distribution of the implanted ions is therefore the same as that in the beam. Note that we are discussing the gaussian profile associated with the focused spot and not that associated with the ion range.

Figure 20a shows an idealised rectangular profile in which a 1 μ m wide stripe is doped to 10^{20} cm⁻³ in a substrate with a background doping concentration of 10^{15} cm⁻³. Also shown are two lateral ion distributions implanted by a gaussian beam with 10% to 90% widths of 1 μ m and 0.5 μ m. The

total doses are chosen to equal the 10^{20} cm^{-3} concentration at the edges of the $1 \mu\text{m}$ stripe. The sample doping is significantly enhanced over approximately a $4 \mu\text{m}$ wide stripe in the case of the $1 \mu\text{m}$ beam and $2 \mu\text{m}$ with the $0.5 \mu\text{m}$ beam. The peak implant dose in the centre of the stripe receives approximately a factor of 20 greater dose than required in the case of the $0.5 \mu\text{m}$ beam. The total number of ions implanted in that case is approximately a factor of 10 greater than in the idealised rectangular masked implant with consequent effects on wafer throughput. In Figures 20b and 20c, the effect of multiple scanning the sample are shown, with 4 adjacent passes of a $0.25 \mu\text{m}$ beam separated by $0.25 \mu\text{m}$ and 8 passes of a $0.125 \mu\text{m}$ beam separated by $0.125 \mu\text{m}$. Clearly the ideal profile is more closely achieved than with single pass implants but, due to the increased number of pixels scanned and the lower current available in the smaller diameter beams, there is a very heavy throughput penalty to pay with this approach. The combination of the gaussian current density profile and the wide range of dopant concentrations encountered in a device mitigates against direct implantation.

A further consideration during implantation is that of dose monitoring and uniformity. In conventional implantation, accurate monitoring of the few milliamps of beam current is relatively easy and good uniformity is achieved by repeated scanning the beam over the sample. In the case of focused ion beams however, accurate dynamic monitoring of the beam would be necessary for high accuracy and good uniformity, this would be very difficult to achieve with the sub nanoamp beam current available.

Ion channeling effects further complicate the use of direct dopant implantation. In conventional implantation, wafers are implanted with the beam incident on the crystal lattice at an angle chosen to minimise ion channeling. The wafers generally employed for device fabrication would show irreproducible ion ranges due to ion channelling if implanted at normal incidence. For direct doping with a focused ion beam this could be overcome either by pre-amorphisation of the wafer or by tilting the wafer and utilising dynamic focusing techniques.

6 MASK FABRICATION AND REPAIR OF MASKS AND DEVICES

Mask fabrication is fundamentally a serial write process and electron beams are widely used to define both optical and X-ray masks. The factors we have discussed concerning the use of ion beams for direct write lithography are directly applicable to mask fabrication. However, ion beams have the capability to modify the properties of the mask material in ways not directly possible with electron beams, consequently they have been studied with a view to using them for mask repair.^{3,4,58,59,60} The throughput limitations associated with focused ion beams are less serious in the case of mask fabrication and particularly mask repair, than in direct-write lithography applications.

Opaque defects in the chrome layer of an optical mask can be cleared by sputtering away unwanted material. Clear defects can be made opaque by ion assisted deposition of material⁵⁹ or by the formation of light deflecting elements, based on diffraction gratings or total internal reflection, within the glass substrate.^{3,4,58,60} Similarly, opaque defects in X-ray masks have been repaired^{3,4} but clear defects pose a much more difficult problem. Focused ion beam systems specifically for mask repair are now commercially available.^{60,61}

The repair of defects on intergrated circuits (IC's) is a further possible application and shares many of the requirements of mask repair.⁶⁰ We have demonstrated the capability to repair the metalisation of an IC by micromachining gaps in the interconnects. Figure 21a shows a micrograph of the interconnect layer of an IC with three breaks in the metalisation formed by machining in the IBL100 with an 80 keV Ga⁺ beam. Figure 21b shows a higher magnification of one of the cut tracks. The growing market for rapid turn-around of ULAs and custom ICs generates its share of incorrectly designed or fabricated devices. A focused ion beam can be used to cut tracks in the metalisation layer to isolate defective areas of a circuit. The modified circuit can then be fully validated before alterations are made to the mask set.

7 MICRO-MACHINING, AMORPHISATION AND ION BEAM MIXING

Focused ion beams may have applications in micro-machining of materials and devices in addition to the mask and device repair already discussed. Micro-machining can either be direct sputtering of the sample by the ions⁶² or can be chemically assisted.^{63,64} The implant doses that are required for direct sputtering are of the order of 10^{18} cm⁻² and this limits the use of micro-machining to small areas of devices. The chemically assisted process requires much lower doses, typically 10^{13} cm⁻². Chemical etching using electron beams to stimulate the system may provide a more versatile "direct-write" etching system offering good lateral resolution as sputtering effects would be absent.

Crystalline silicon can be amorphised by ion implantation thereby changing many of its properties. For example, amorphous silicon is preferentially etched by hydrofluoric acid and it has high electrical resistivity. The doses required for amorphisation are generally around 10^{14} ions cm⁻².

Focused ion beams could be used for ion beam mixing of metal layers deposited on silicon for silicide formation.⁶⁵ The implant may be of a doping or an inert species with a dose of approximately 5×10^{14} cm⁻².⁶⁴

8 CONCLUSIONS

Resists for lithography applications are more sensitive to exposure to ion beams than to electron beams. In practice this does not translate into increased wafer throughput for direct-write lithography for a number of reasons. Firstly, the current density available for resist exposure from a LMIS is less than that from electron sources, typically by a factor of approximately 100. This effectively negates the resist sensitivity advantage of ions. Secondly, the shaped beam and multi-beam approaches to increased throughput in electron beam columns are not applicable to LMIS based columns due to the lower available current from LMIS. Thirdly, statistical fluctuations in the beam current place an upper limit on the resist sensitivities that can be used. An advantage that ion beams have over the low energy electron beams currently used for direct write lithography is their freedom from the proximity effect. However, the proximity effect with electron beams can be greatly reduced by using higher accelerating voltages. Layer-to-layer alignment currently remains a major unsolved problem with ion beam lithography. For ultra-fine lithography, ion beams are not appropriate; electron sources and optics are capable of producing much smaller spot sizes. We conclude that electron beams are a

better choice than ion beams for direct-write lithography.

Direct doping is not capable of high throughput device production. It can, however, provide control of the lateral doping profile which is not easily achieved by any other method. Direct doping may be of interest for the fabrication of individual experimental devices but its use is severely restricted by its low throughput and the difficulty of achieving large dopant concentration gradients with the gaussian beams available.

Ion beams may be of use for optical mask making but the comments about ion beam systems and throughput for lithography applications apply equally here. Ion beam systems are now commercially available for mask repair but must compete with the present laser based systems.⁶⁶ However, mask repair would appear to be the first and most likely commercial application of focused ion beams. Their application to circuit repair is also very exciting and is receiving attention⁶⁰ but this also faces competition from laser based systems⁶⁷ which have the advantage of economics. Micro-machining and amorphisation may find specific niches but in general, focused ion beams are not a unique solution to micro-machining problems.

Over recent years, focused ion beams have appeared to offer great potential in a number of areas. Unfortunately, close examination of each of these applications has shown that their early promise will not be fulfilled. In practice, there are significant problems, both physical and technological which mitigate against their use in device fabrication except under very restricted circumstances. Despite this, it is most regrettable that the VG IBL100 contained so many design faults and that so little support for its improvements was forthcoming. Because of this, we were unable to answer a number of the outstanding questions that we have discussed.

REFERENCES

- 1 H Ryssel and K Habeger, in "Microcircuit Engineering 81" (Proceedings of the International Conference on Microlithography, Lausanne, Switzerland, 1981), pp. 299.
- 2 W L Brown, T Venkatesan and A Wagner, Solid State Technology, 24(8), 60 (1981).
- 3 A Wagner, Solid State Technology, 26(5), 97 (1983).
- 4 W L Brown and A Wagner, Proc. Int'l. Ion Engineering Congress - ISIAAT'83 and IPAT'83, Kyoto, Japan (1983), pp. 1738A.
- 5 S Namba, Proc. Int'l. Ion Engineering Congress - ISIAAT'83 and IPAT'83, Kyoto, Japan (1983), pp. 1533.
- 6 H Shearer and G Cogswell, Semiconductor International, 7(4), 145 (1984).
- 7 R L Seliger, J W Ward, V Wang and R L Kubena, Appl. Phys. Lett. 34, 310 (1979).

- 8 L Swanson, in "Microcircuit Engineering 80", Ed. R P Kramer (Delft University Press, Delft, The Netherlands, 1981), pp. 267.
- 9 J R A Cleaver and H Ahmed, J. Vac. Sci. Technol. 19, 1145 (1981).
- 10 J Orloff and L W Swanson, J. Vac. Sci. Technol. 19, 1149 (1981).
- 11 V Wang, J W Ward and R L Seliger, J. Vac. Sci. Technol. 19, 1158 (1981).
- 12 R Levi-Setti, T R Fox and K Lam, Nucl. Instrum. Methods. 205, 299 (1983).
- 13 T Shiokawa, P H Kim, K Toyoda, S Namba and K Gamo. J. Vac. Sci. Technol. B 1, 1117 (1983).
- 14 T Ishitani, K Umemura and H Tamura, Nucl. Instrum. Methods. 218, 363 (1983).
- 15 K Komagata, O Tsukakoshi, T Katagawa and S Komiya, Proc. Int'l. Ion Engineering Congress - ISIAT'83 & IPAT'83, Kyoto, Japan (1983), pp. 781.
- 16 R J Blackwell, J A Kubby, G N Lewis and B M Siegel, J. Vac. Sci. Technol. B 3, 82 (1985).
- 17 T Itakura, K Horiuchi and S Yamamoto, in "Microcircuit Engineering 85", Ed. K D van der Mast and S Radelaar (North-Holland Publishing Co. The Netherlands, 1985), pp. 153.
- 18 G Dearnaley, J H Freeman, R S Nelson and J Stephen, "Ion Implantation" (North-Holland Publishing Co. The Netherlands, 1973), pp. 292-386.
- 19 G L R Mair and T Mulvey, Scanning Electron Microscopy, 4, 1531 (1984).
- 20 G L R Mair and T Mulvey, in "Microcircuit Engineering 85", Ed. K D van der Mast and S Radelaar (North-Holland Publishing Co. The Netherlands, 1985), pp. 133.
- 21 G L R Mair and T Mulvey, Scanning Electron Microscopy, 3, 959 (1985).
- 22 H C Pfeiffer, in "Microcircuit Engineering 83", Ed. H Ahmed, J R A Cleaver and G A C Jones (Academic Press, 1983), pp. 3.
- 23 A N Broers, Solid State Technology, 28(6), 119 (1985).
- 24 K Kurihara, J. Vac. Sci. Technol. B 3, 41 (1985).
- 25 G R Hanson and B M Siegel, J. Vac. Sci. Technol. 16, 1875 (1979).
- 26 B M Siegel, G R Hanson, M Szilagyí, D R Thomas, R J Blackwell, H Paik, S.P.I.E. 333, 152 (1982).
- 27 J Orloff and P Sudraud, in "Microcircuit Engineering 85", Ed. K D van der Mast and S Radelaar (North-Holland Publishing Co. The Netherlands, 1985), pp. 161.

- 28 J Benjamin and J White in "Microcircuit Engineering 85", Ed. K D van der Mast and S Radelaar (North-Holland Publishing Co. The Netherlands, 1985), pp. 235.
- 29 J S Greeneich, "Electron-Beam Processes" in "Electron-Beam Tecnology In Microelectronic Fabrication", Ed G R Brewer (Academic Press, 1980), pp. 60-141.
- 30 R E Howard, H G Craighead, L D Jackel, P M Mankiewich and M Feldman, J. Vac. Sci. Technol. B 1, 1101 (1983).
- 31 A N Broers, J. Electrochem. Soc. 128, 166 (1981).
- 32 T M Hall, A Wagner and L F Thompson, J. Vac. Sci. Technol. 16, 1889 (1979).
- 33 I Adesida, E Kratschmer, E D Wolf, A Muray and M Isaacson, J. Vac. Sci. Technol. B 3, 45 (1985).
- 34 R G Brault and L J Miller, Polymer Engineering and Science, 20, 1064 (1980).
- 35 M Komuro, N Atoda and H Kawakatsu, J Electrochem. Soc. 126, 483 (1979).
- 36 H Ryssel, K Haberger and H Kranz, J. Vac. Sci. Technol. 19, 1358 (1981).
- 37 R G Brault, R L Kubena and J E Jensen, Polymer Enginnering and Science, 23, 941 (1983).
- 38 I Adesida, C Anderson and E D Wolf, J. Vac. Sci. Technol. B 1, 1182 (1983).
- 39 I Adesida, M Zhang, E D Wolf, J Electronic Materials, 13, 689 (1984).
- 40 N Chan Tung, J Electrochem. Soc., 131, 2152 (1984).
- 41 A Macrander, D Barr, A Wagner, S.P.I.E. 333, 142 (1982).
- 42 J R A Cleaver, P J Heard and H Ahmed, in "Microcircuit Engineering 82" (Proceedings of the International Conference on Microlithography, Grenoble, France, 1982), pp. 148.
- 43 H S Carslaw and J C Jaeger, "Conduction of Heat in Solids", 2nd edition (Oxford University Press, 1973).
- 44 A G Brown, S H Mortimer S J Till and V G I Deshmukh, in "Microcircuit Engineering 85", Ed. K D van der Mast and S Radelaar (North-Holland Publishing Co. The Netherlands, 1985), pp. 443.
- 45 H Kuwano, K Yoshida and S Yamazaki, Jpn. J. Appl. Phys. 19, L615 (1980).
- 46 J E Jenson, Solid State Technology, 27(6), 145 (1984).
- 47 H Kuwano, J. Appl. Phys. 55, 1149 (1984).

- 48 T Venkatesan, G N Taylor, A Wagner, B Wilkens and D Barr, J. Vac. Sci. Technol. 19, 1379 (1981).
- 49 I Adesida, J D Chinn, L Rathbun and E D Wolf, J. Vac. Sci. Technol. 21, 666 (1982).
- 50 R L Kubena, C L Anderson, R L Seliger, R A Jullens, E H Stevens and I Lugnado, J. Vac. Sci. Technol. 19, 916 (1981).
- 51 R L Seliger, R L Kubena and V Wang, Jpn. J. Appl. Phys. 21, Supplement 21-1, 3 (1982).
- 52 Y Bamba, E Miyauchi, H Arimoto, K Kuramoto, A Takamori and H Hashimoto, Jpn. J. Appl. Phys. 22, L650 (1983).
- 53 Y Bamba, E Miyauchi, H Arimoto, K Kuramoto, A Takamori and H Hashimoto, Jpn. J. Appl. Phys. 23, L515 (1984).
- 54 R H Reuss, D Morgan, E W Greeneich, W M Clark, Jr and D B Rensch, J. Vac. Sci. Technol. B 3, 62 (1985).
- 55 H Hamadeh, J C Corelli and A J Steckl, J. Vac. Sci. Technol. B 3, 91 (1985).
- 56 M Tamura, S Shukuri, S Tachi, T Ishitani and H Tamura, Jpn. J. Appl. Phys. 22, L700 (1983).
- 57 M Tamura, S Shukuri, T Ishitani, M Ichikawa and T Doi, Jpn. J. Appl. Phys. 23, L417 (1984).
- 58 P J Heard, J R A Cleaver and H Ahmed, J. Vac. Sci. Technol. B 3, 87 (1985).
- 59 J R A Cleaver, H Ahmed, P J Heard, P D Prewett, G J Dunn and H Kaufmann, in "Microcircuit Engineering 85", Ed. K D van der Mast and S Radelaar (North-Holland Publishing Co. The Netherlands, 1985), pp. 253.
- 60 D C Shaver and B W Ward, Solid State Technology 28(12), 73 (1985).
- 61 Ion Beam Technologies, 123 Brimbal Avenue ,Beverly, MA. USA.
- 62 H Yamaguchi, A Shimase, S Haraichi and T Miyauchi, J. Vac. Sci. Technol. B 3, 71 (1985).
- 63 Y Ochiai, K Gamo, S Namba, J. Vac. Sci. Technol. B 1, 1047 (1983).
- 64 Y Ochiai, K Gamo, S amba, J. Vac. Sci. Technol. B 3, 67 (1985).
- 65 W F Van der Weg, D Sigurd and J W Mayer, in S T Picraux, E P EerNisse and F Vook, "Applications of Ion Beams to Metals", (Plenum, New York, 1976), pp. 209.
- 66 Quantronix Corporation, 225 Engineers Road, Smithtown, New York 11788.
- 67 D J Ehrlich, Solid State Technology 28(12), 81 (1985).

FIGURE TITLES

Figure 1. Schematic diagram of VG IBL100 focused ion beam implanter column.

Figure 2. Schematic diagram of RSRE pattern generation system.

Figure 3. a) Bright-field transmission electron micrograph of the cross-sections of amorphous lines in single crystal silicon generated by 80 keV Ga⁺ ion implants at five different doses. b) An enlargement of the widest stripe of 3a).

Figure 4. Dose versus linewidth as measured from figure 3a).

Figure 5. Secondary electron yield (arbitrary units) as a function of beam position as it is scanned over a sharp silicon wedged edge.

Figure 6. Exposure time (per 80 mm²) versus resist sensitivity for beam current densities of 1 A cm⁻² and 100 A cm⁻².

Figure 7. Exposure time (per 80 mm²) versus pixel dimension at three resist sensitivities assuming a beam current density of 100 A cm⁻².

Figure 8. Minimum pixel dimension as a function of resist sensitivity for three values of N.

Figure 9. Surface topography generated by ion beam heating of PMMA. Approximate doses and beam current densities are a) 3×10^{15} ions cm⁻² at 20 A cm⁻² b) 2.4×10^{15} ions cm⁻² at 3 A cm⁻² c) 1×10^{15} ions cm⁻² at 9 A cm⁻² d) 1×10^{15} ions cm⁻² at 3 A cm⁻² e) & f) 3.6×10^{14} ions cm⁻² at 20 A cm⁻² g) 2.3×10^{14} ions cm⁻² at 9 A cm⁻² h) 1.5×10^{14} ions cm⁻² at 0.8 A cm⁻²

Figure 10. Maximum beam dwell time (to prevent resist over heating) as a function of beam current density for an ion beam of 80 keV Ga⁺ and spot size 1750 Å.

Figure 11. Residual gas mass spectrum of a) the background atmosphere of the IBL100 and b) the IBL100 atmosphere while exposing PMMA.

Figure 12. Partial pressure of mass 16 as a function of dose during exposure in the IBL100 at a dose rate of 4×10^{14} ions cm⁻² s⁻¹.

Figure 13. Partial pressure of mass 16 as a function of dose during exposure in the IBL100 at a dose rate of 2.7×10^{13} ions cm⁻² s⁻¹.

Figure 14. PMMA thickness loss as a function of dry etching time after implantation with 40 keV Ga.

Figure 15. PMMA thickness loss as a function of dry etching time after implantation with 180 keV Ga.

Figure 16. PMMA thickness loss as a function of dry etching time after Ga⁺, Ar⁺, B⁺, H⁺ and electron implants.

Figure 17. Infra-red absorption spectrum (Relative transmittance versus wave number) for untreated PMMA.

Figure 18. Infra-red absorption spectrum (Relative transmittance versus wave number) for PMMA implanted with 10^{15} Ga⁺ 100 keV ions cm⁻²

Figure 19. Features delineated on the IBL100 and subsequently dry etched.

Figure 20. Doping density profiles produced by a) a single pass of a $1\ \mu\text{m}$ (10%-90%) and $0.5\ \mu\text{m}$ (10%-90%) beam, b) 4 passes of a $0.25\ \mu\text{m}$ (10%-90%) beam and c) 8 passes of a $0.125\ \mu\text{m}$ (10%-90%) beam compared with an ideal $1\ \mu\text{m}$ profile.

Figure 21a) A micrograph of the metalisation layer of an integrated circuit within which three tracks have been cut by direct micromachining with a focused ion beam in the IBL100. b) An enlargement of one of the breaks in the metal tracks.

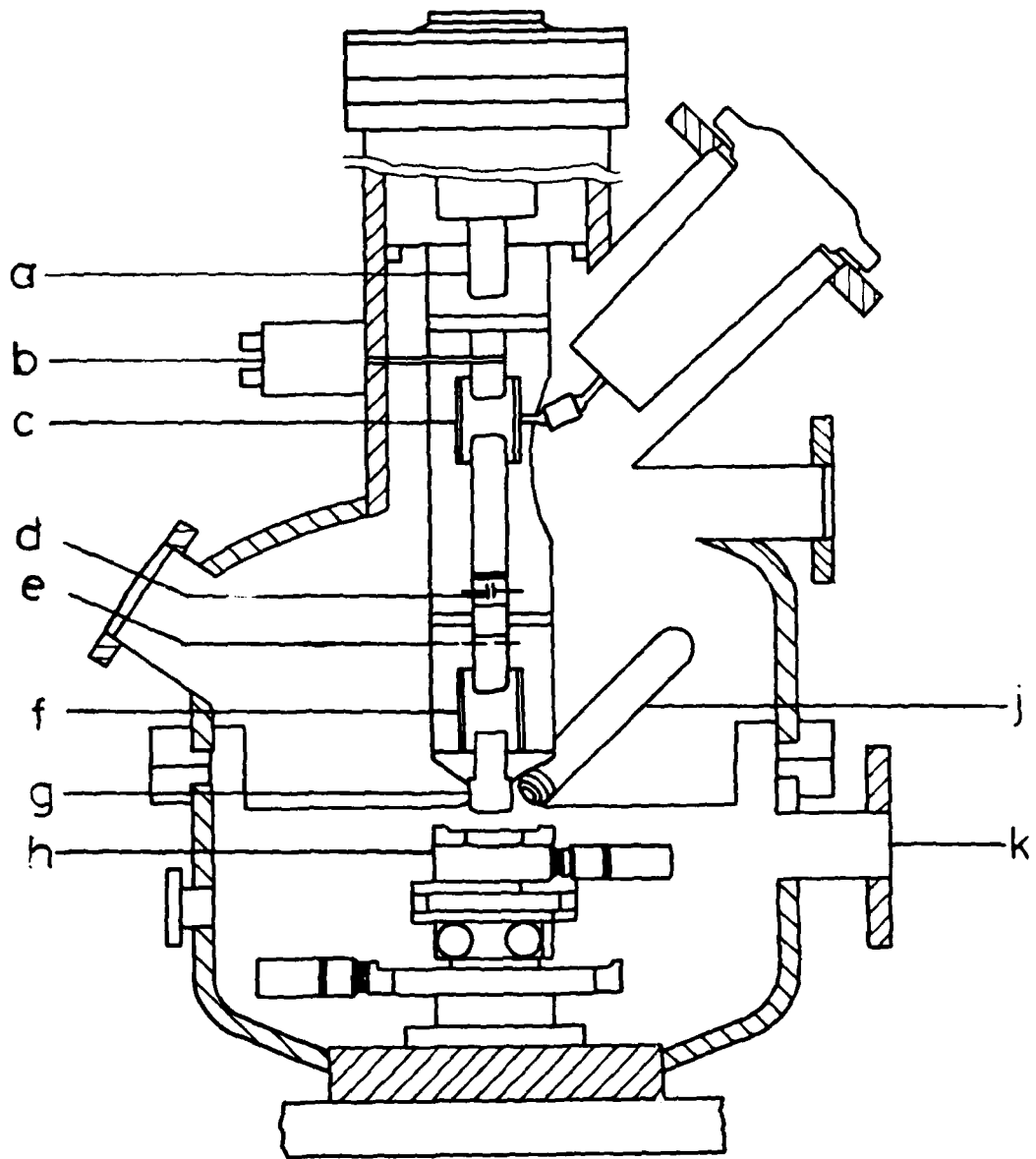


FIGURE 1

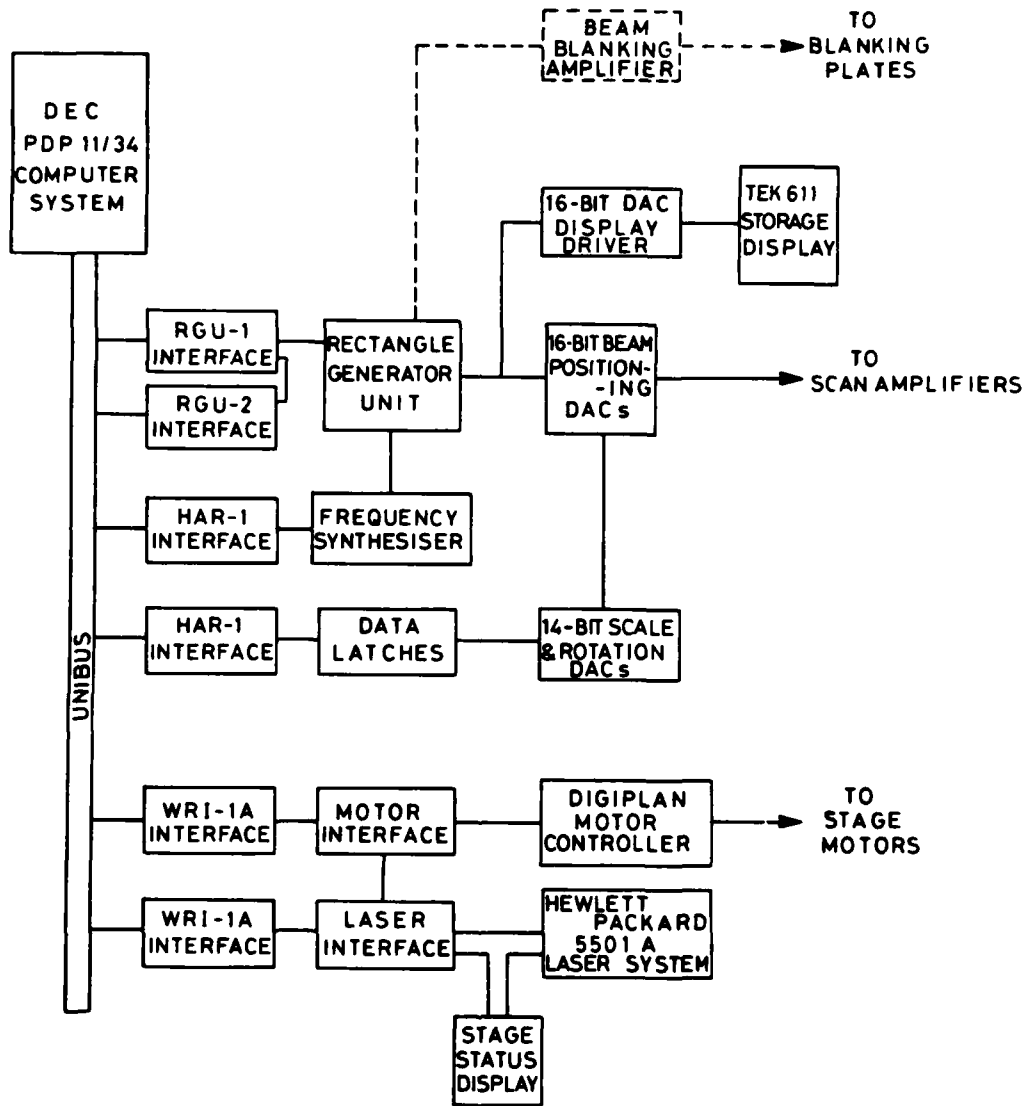


FIGURE 2

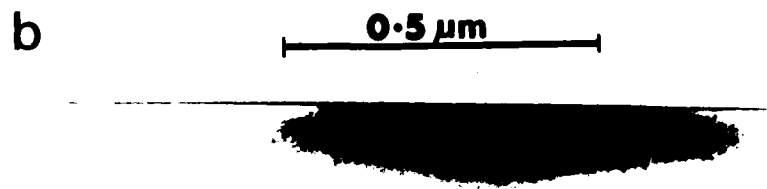
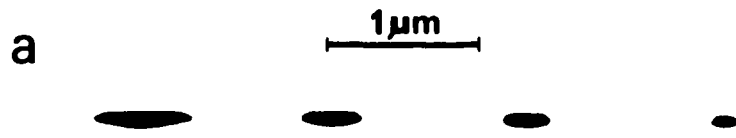


FIGURE 3

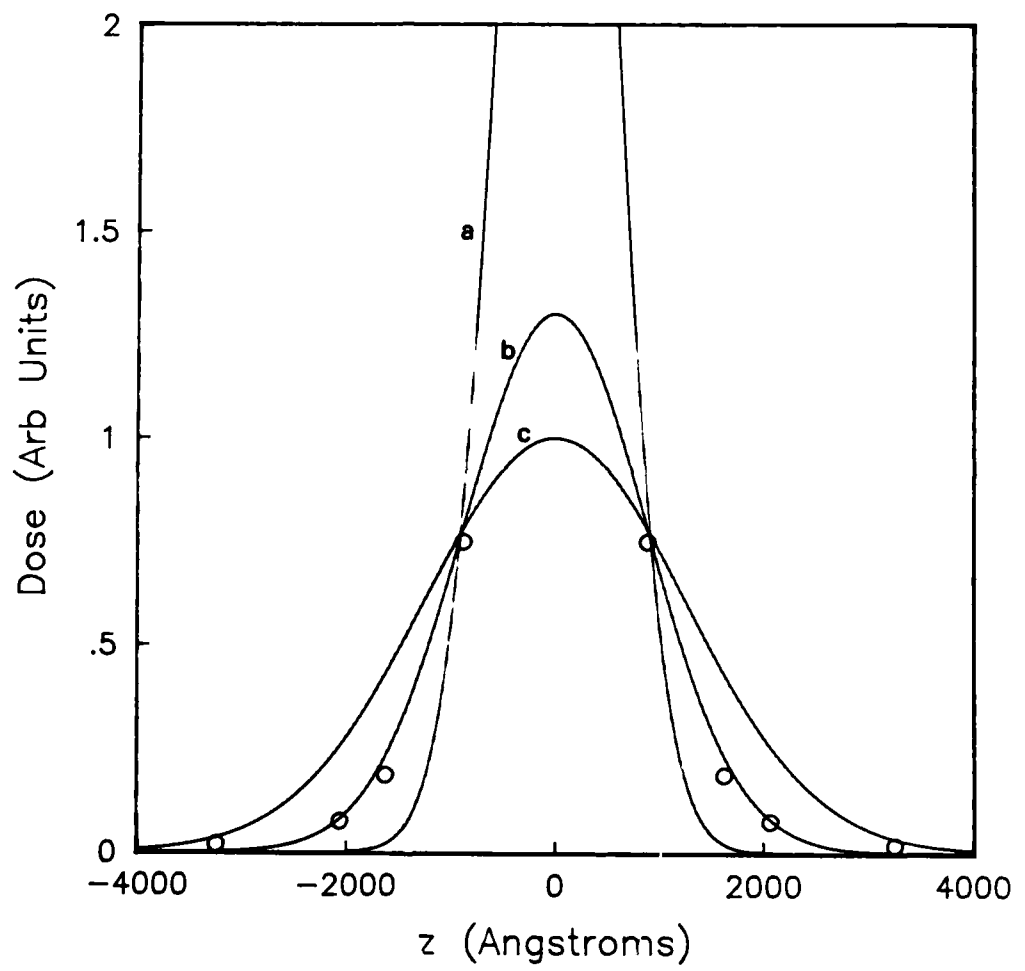


FIGURE 4

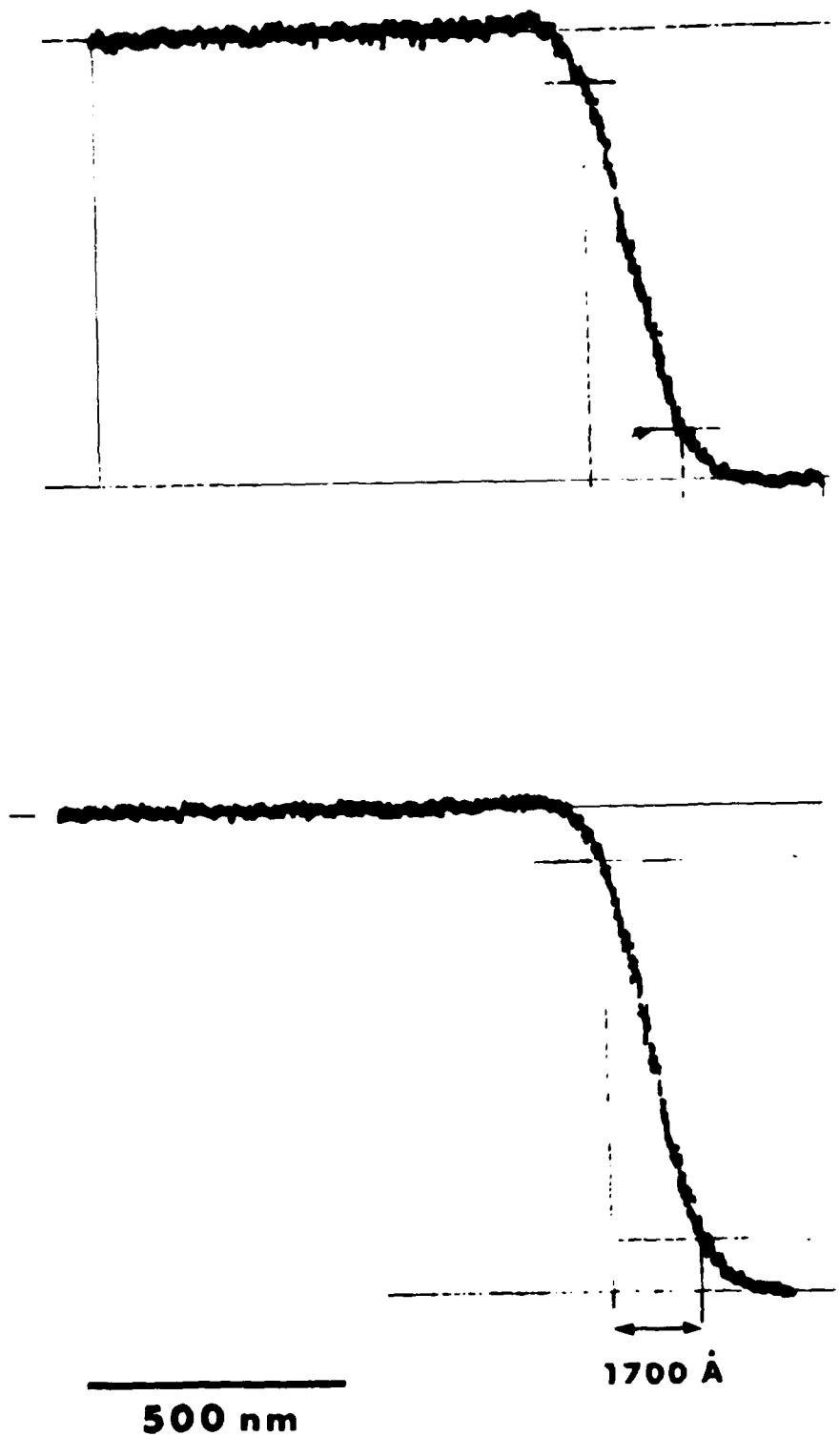


FIGURE 5

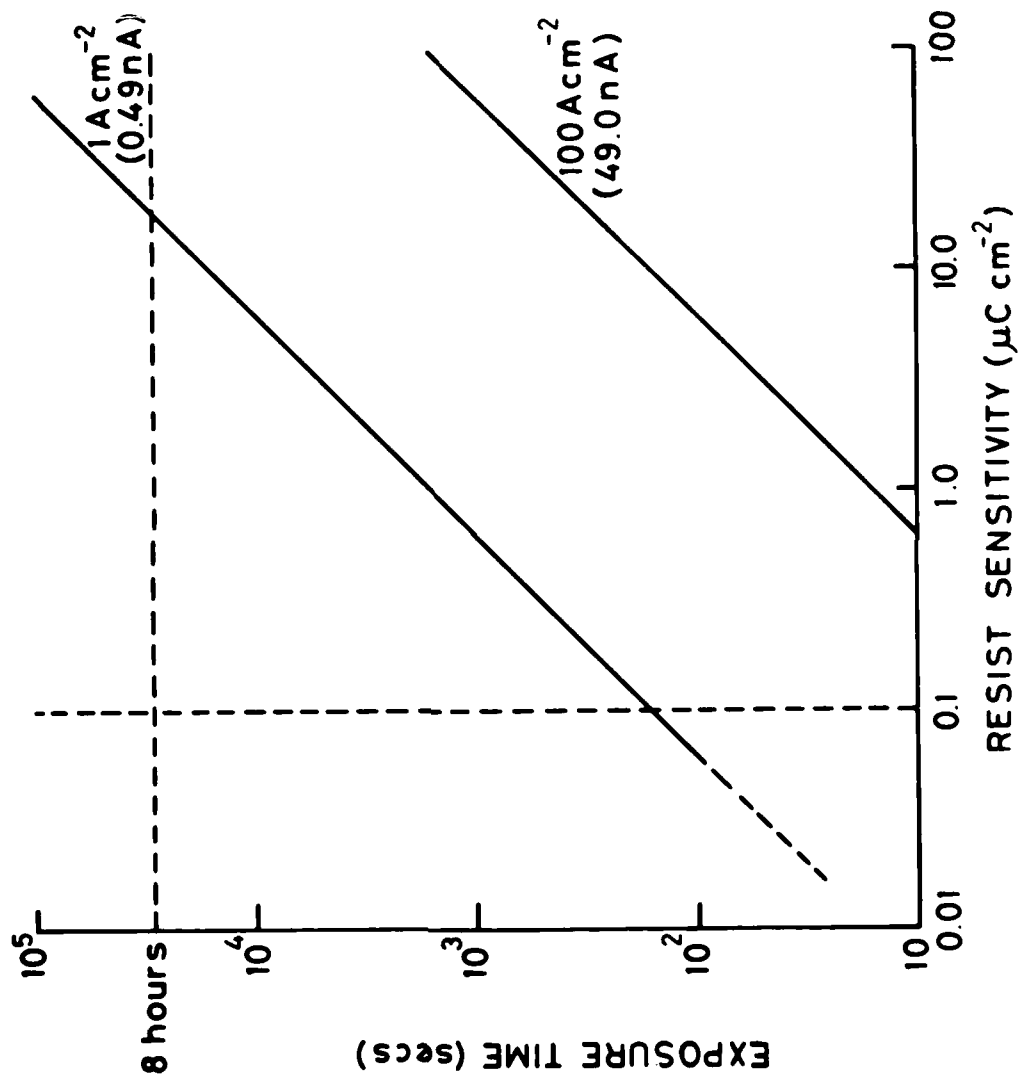


FIGURE 6

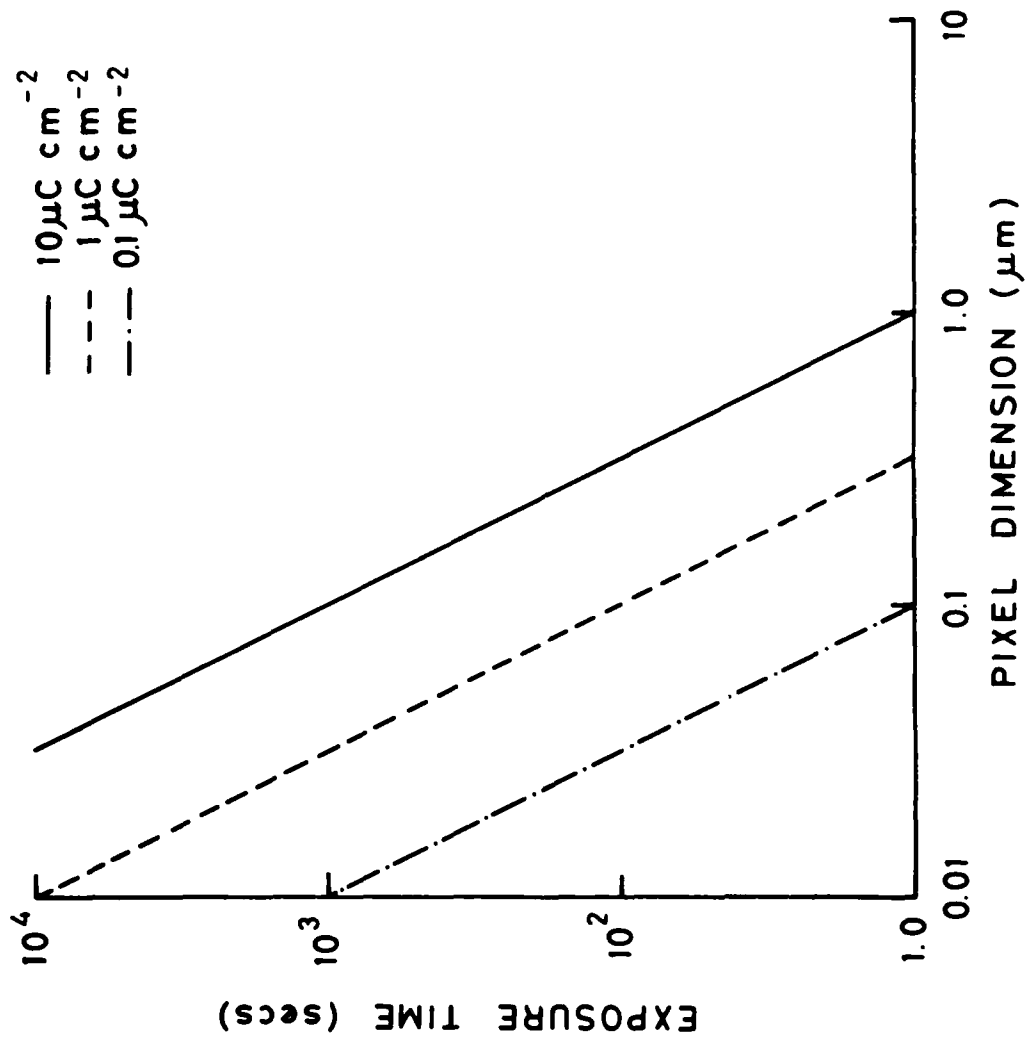


FIGURE 7

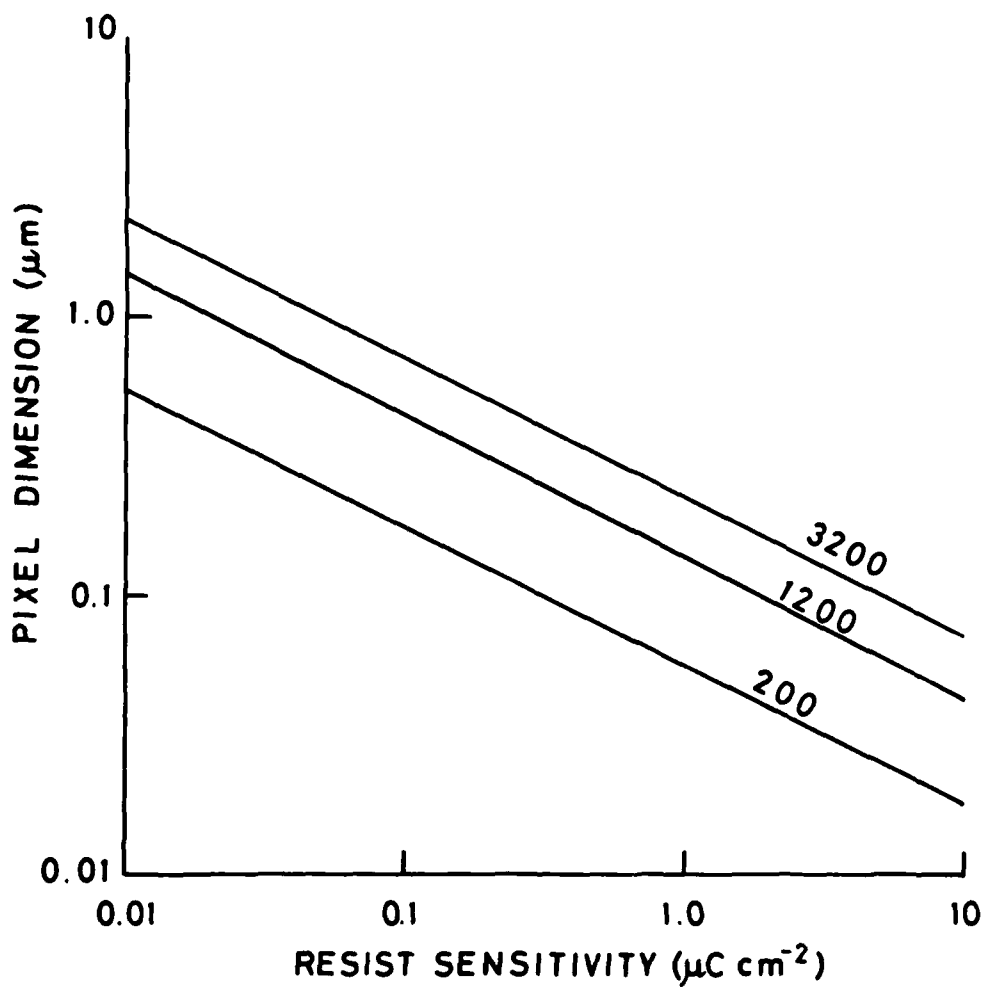
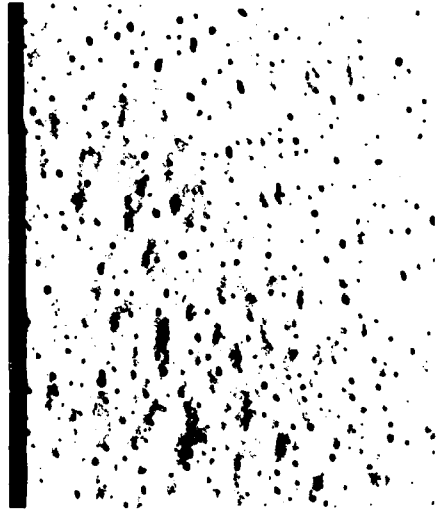


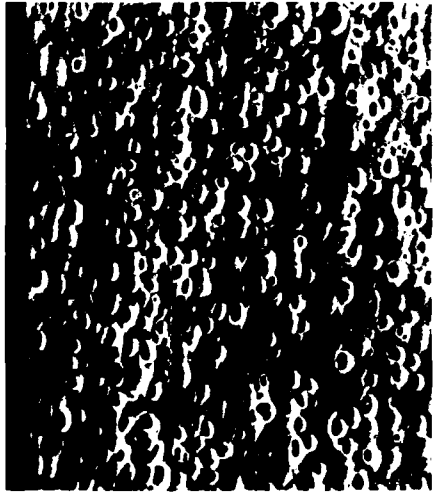
FIGURE 8



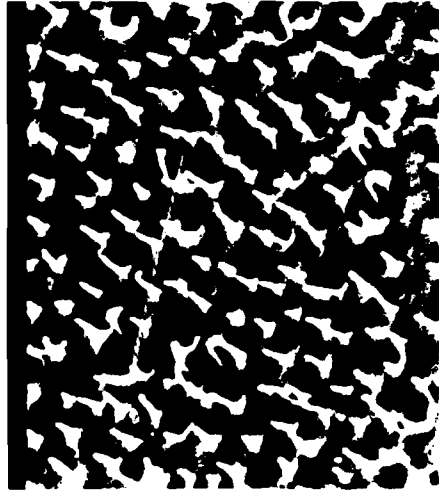
b



d



a

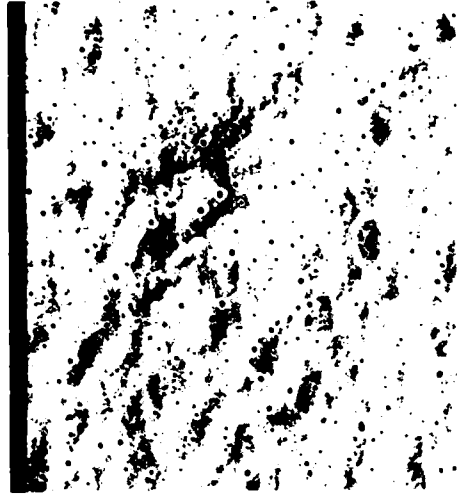


c

FIGURE 9



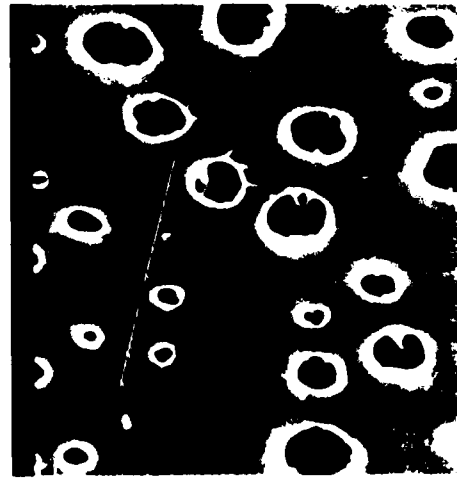
f



h



e



g

FIGURE 9

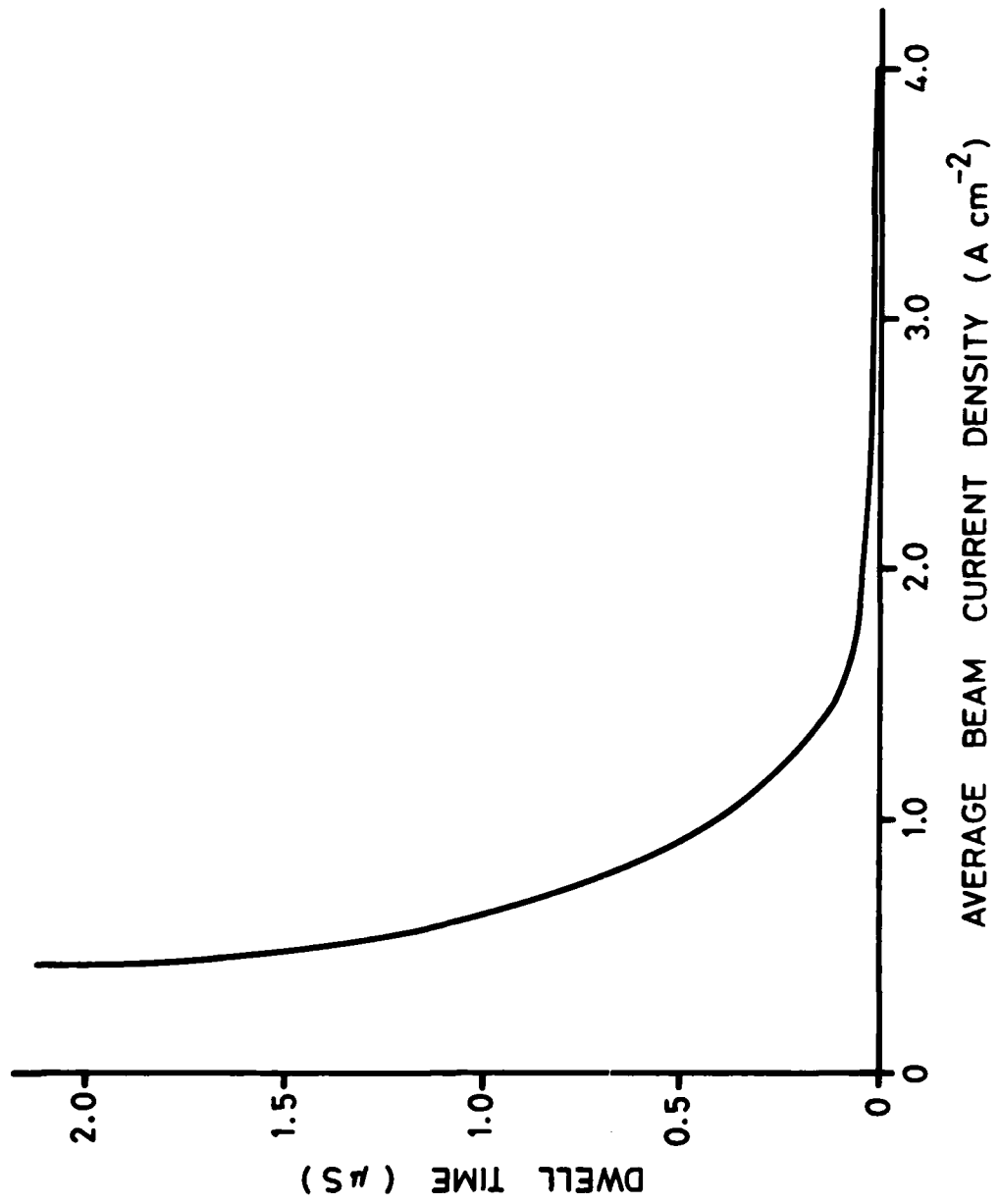


FIGURE 10

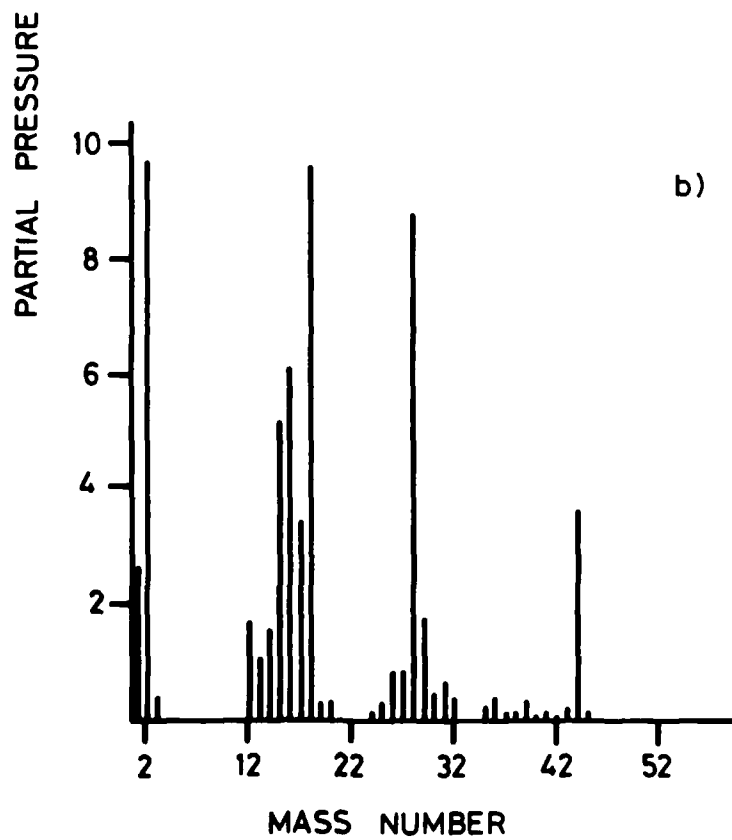
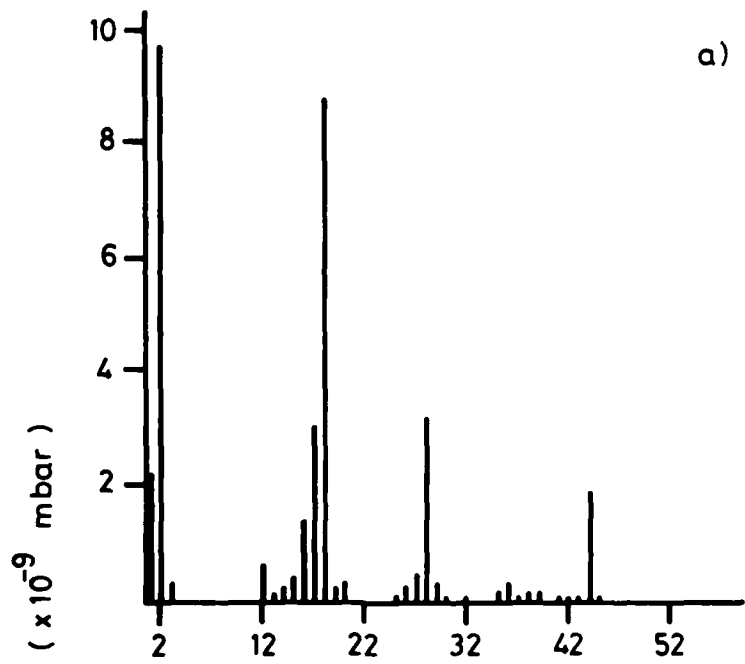


FIGURE 11

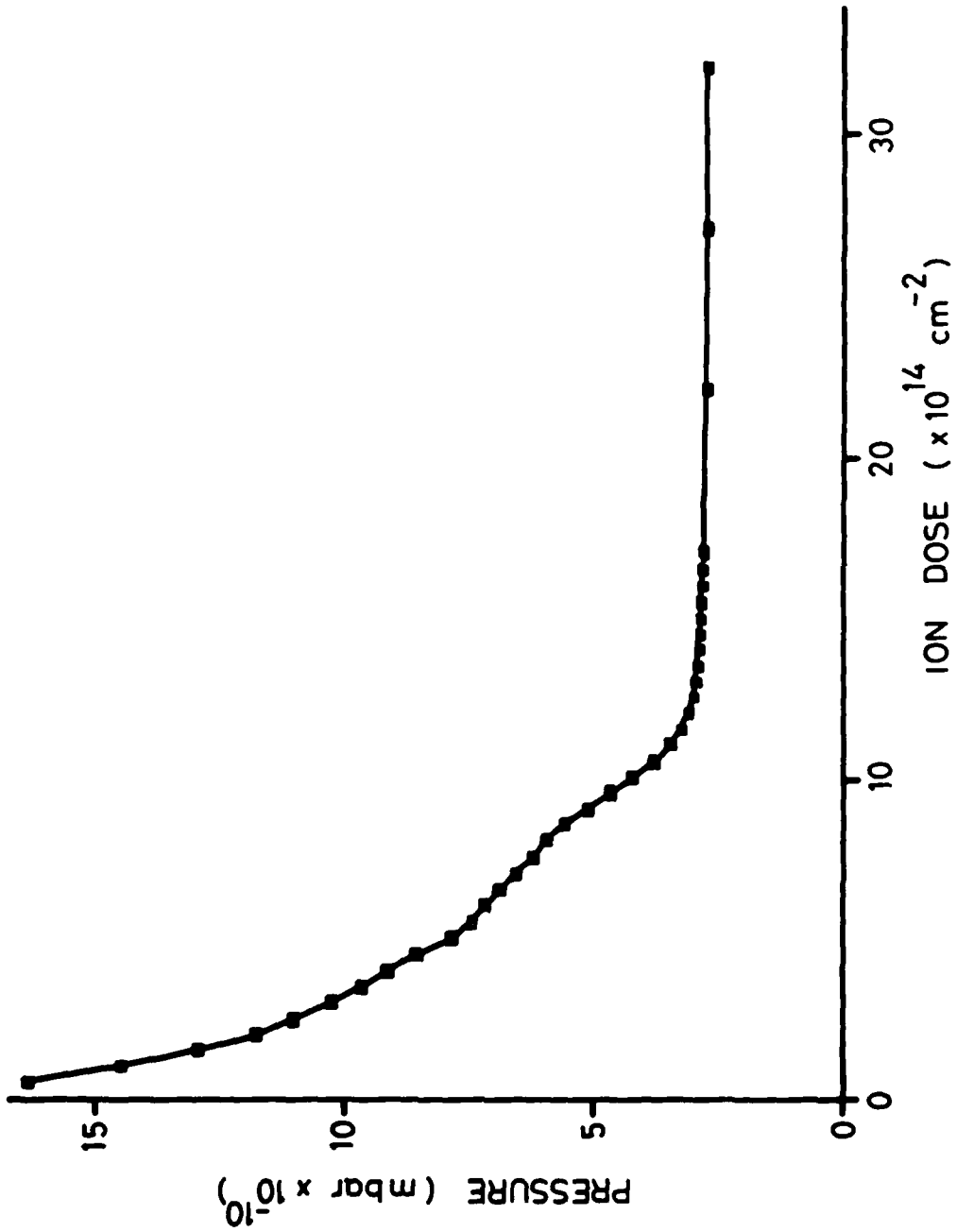


FIGURE 12

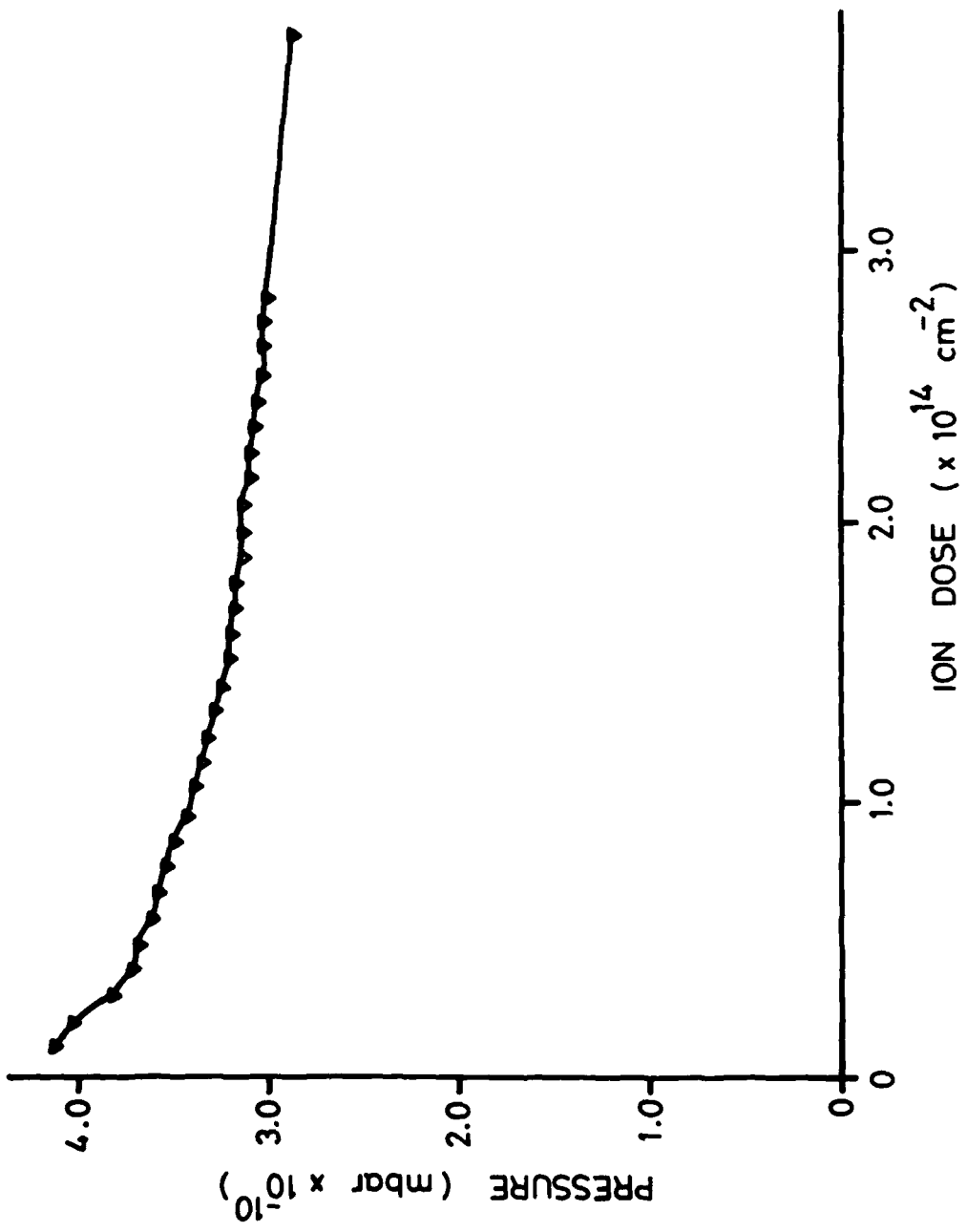


FIGURE 13

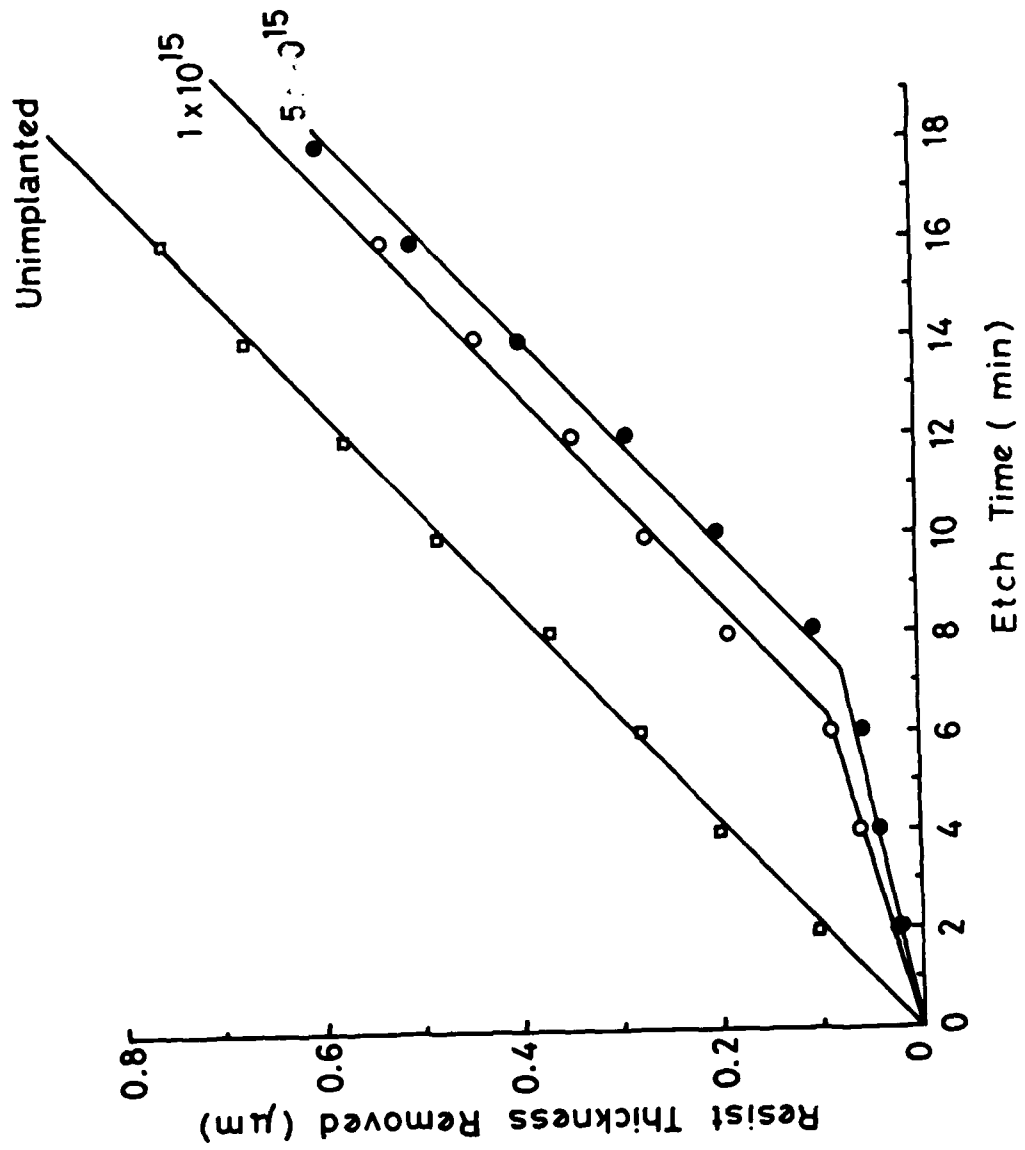


FIGURE 14

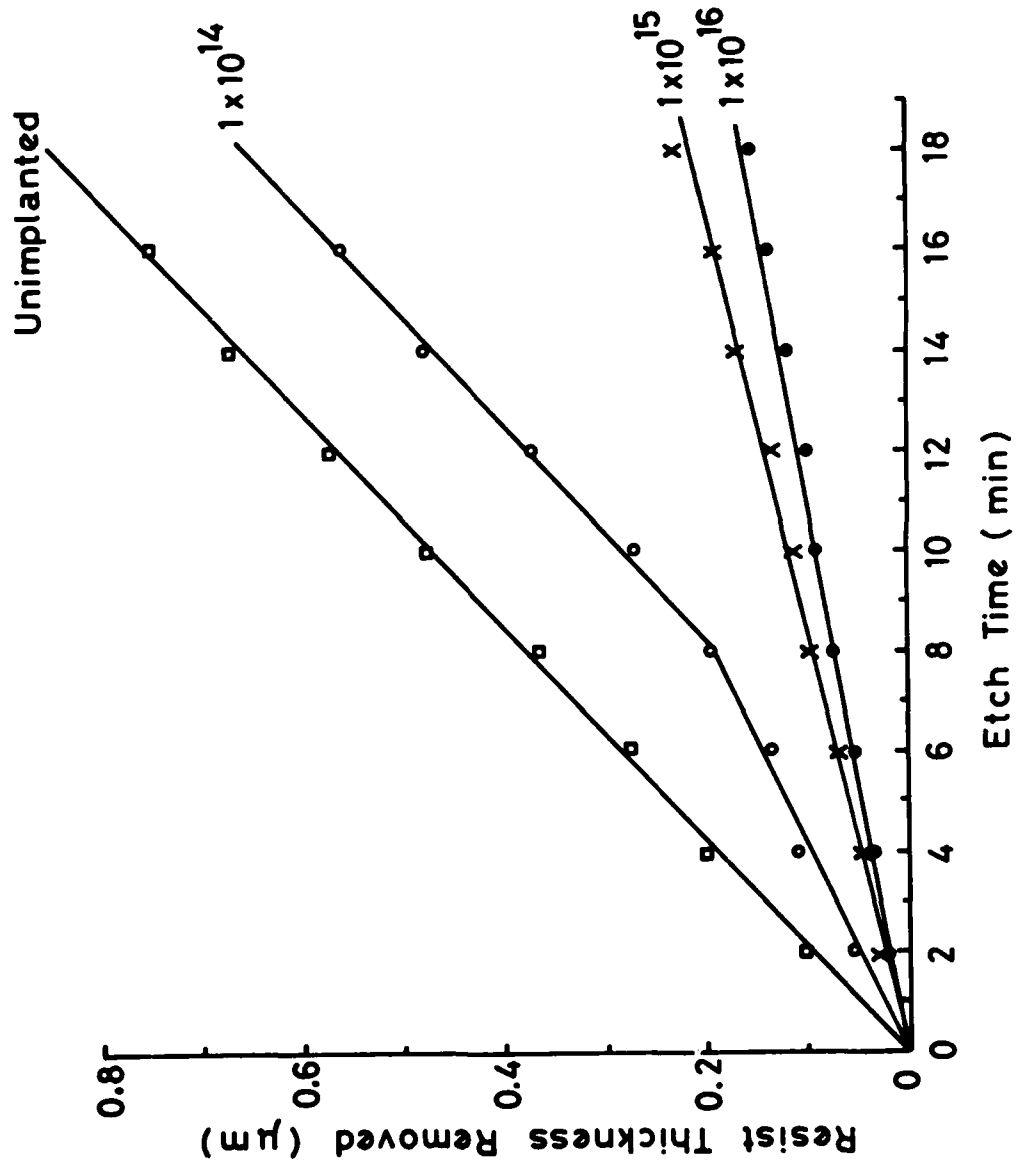


FIGURE 15

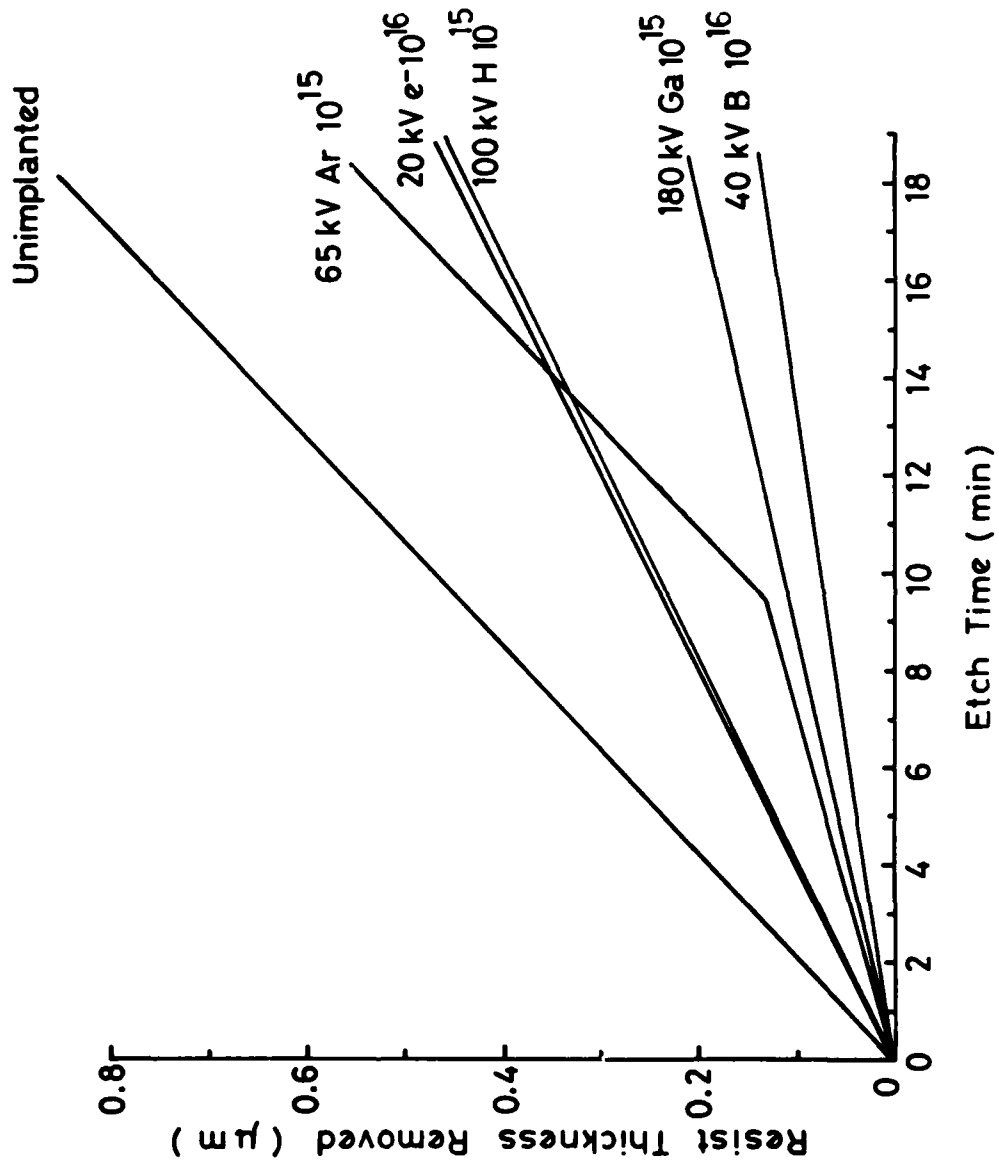


FIGURE 16

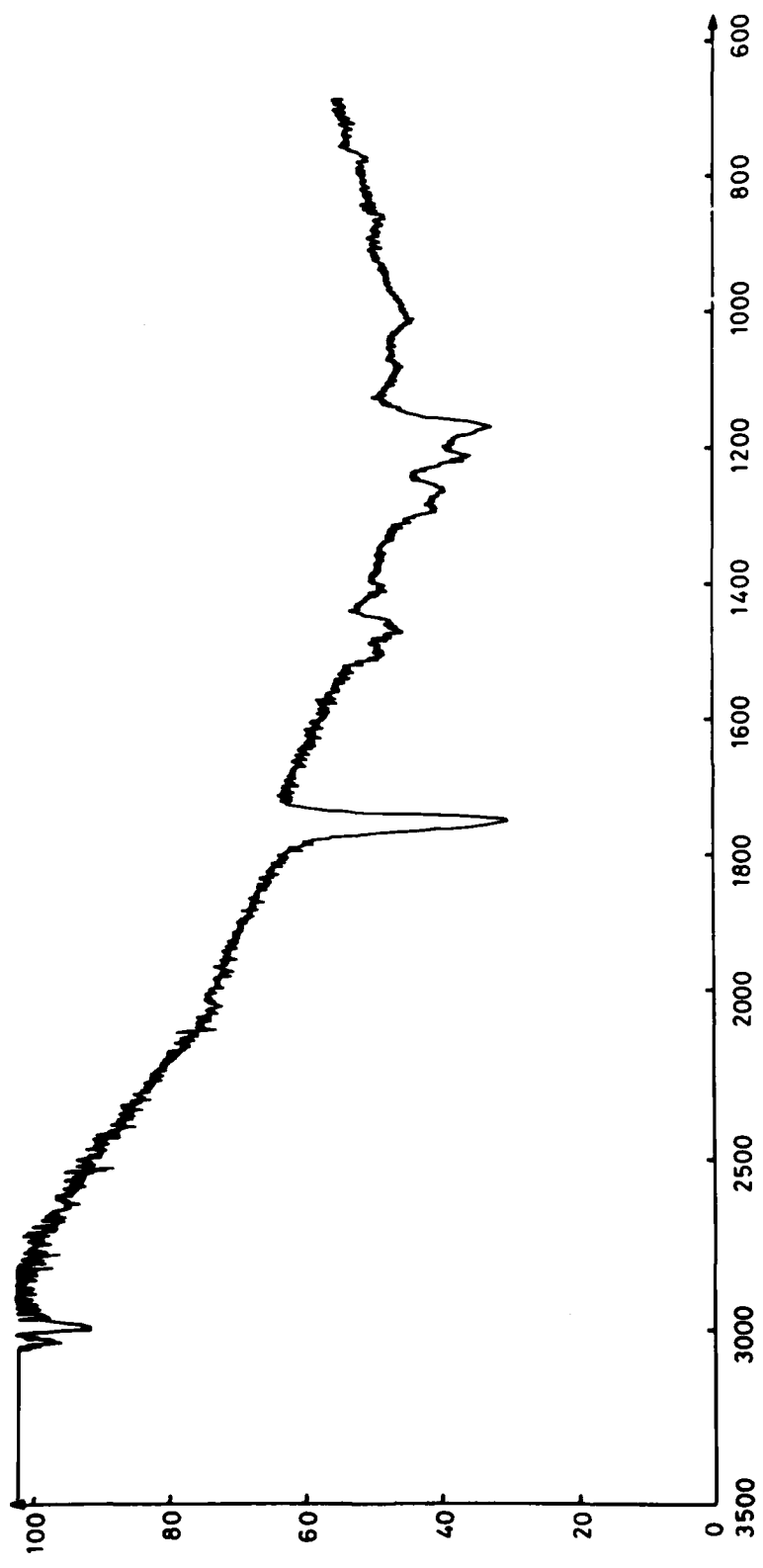


FIGURE 17

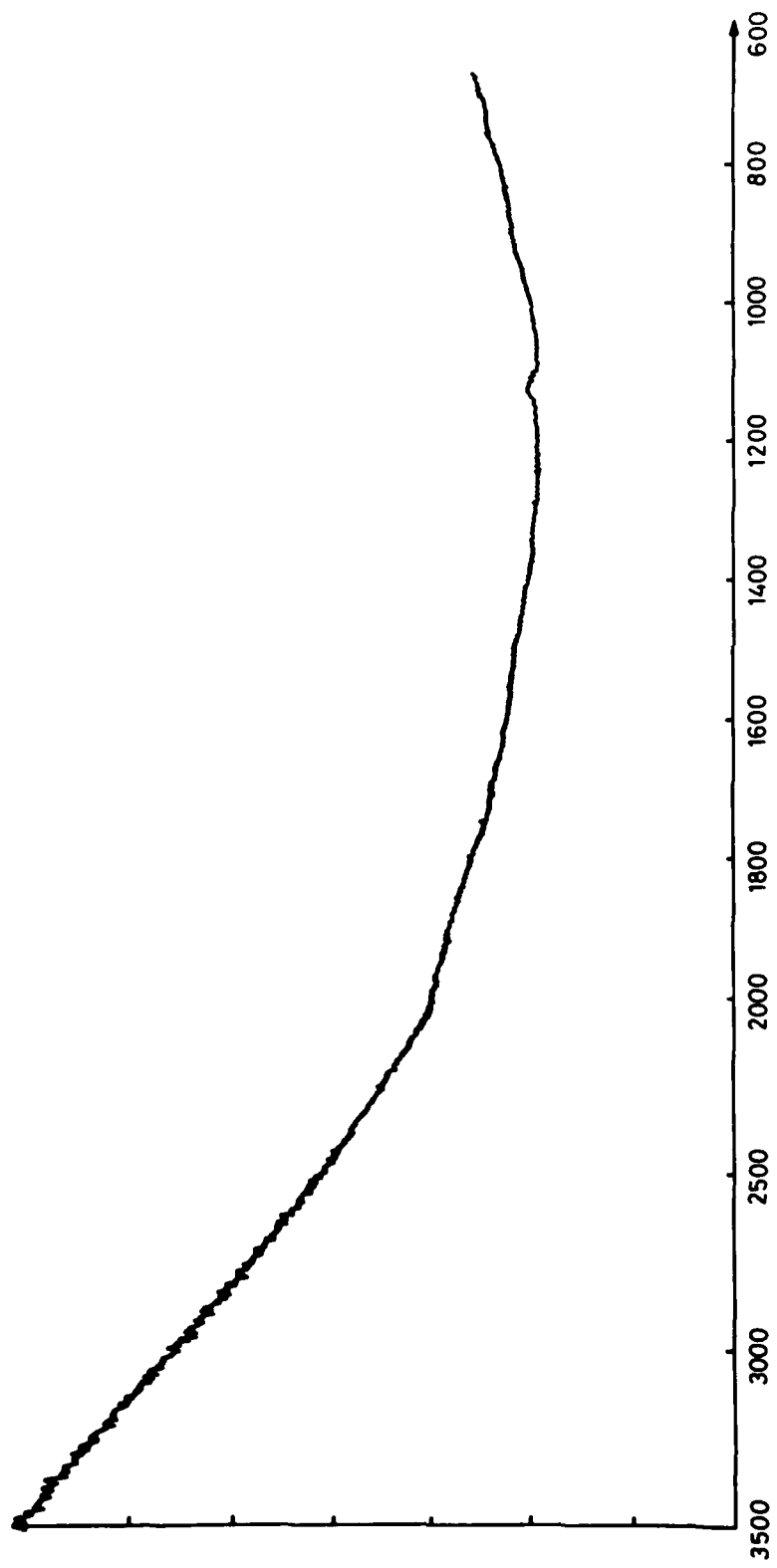


FIGURE 18



a



b



c



d

FIGURE 19

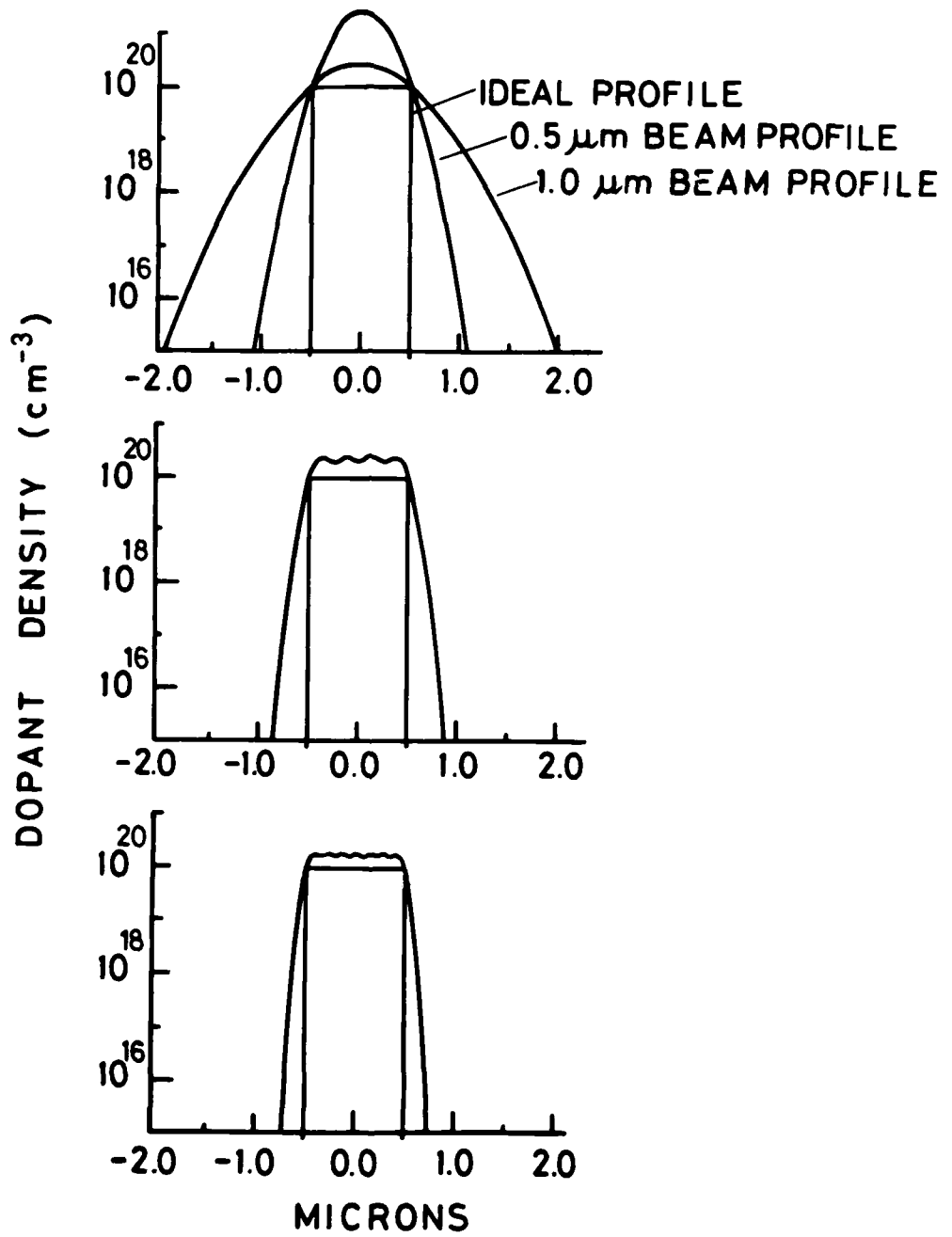
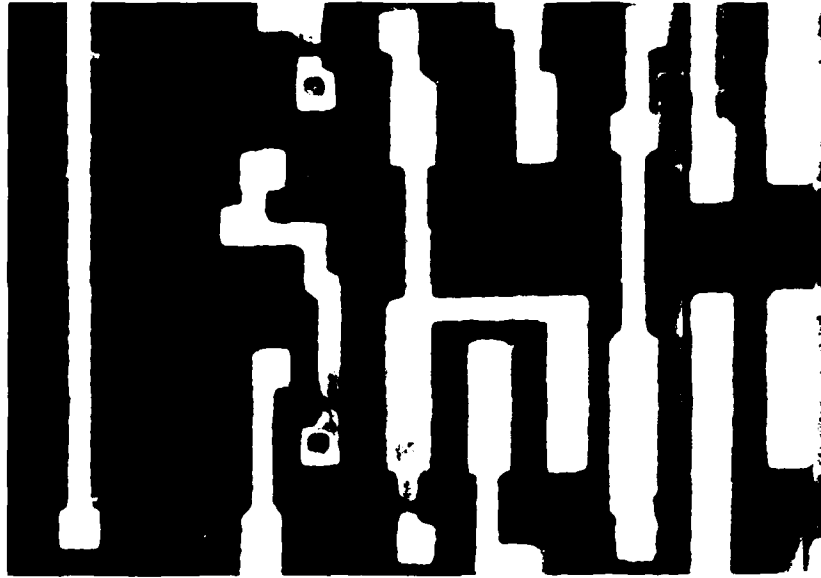


FIGURE 20

a)

50 μm



b)

5 μm

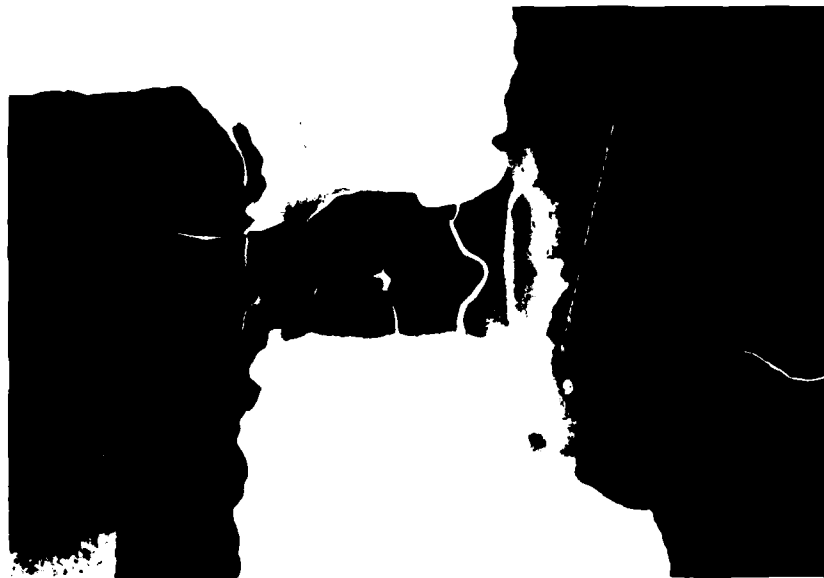


FIGURE 21

DOCUMENT CONTROL SHEET

Overall security classification of sheet UNCLASSIFIED

(As far as possible this sheet should contain only unclassified information. If it is necessary to enter classified information, the box concerned must be marked to indicate the classification eg (R) (C) or (S))

1. DRIC Reference (if known)	2. Originator's Reference Memorandum 3948	3. Agency Reference	4. Report Security Classification U/C	
5. Originator's Code (if known)	6. Originator (Corporate Author) Name and Location Royal Signals and Radar Establishment			
5a. Sponsoring Agency's Code (if known)	6a. Sponsoring Agency (Contract Authority) Name and Location			
7. Title Applications of focused ion beams in microelectronics				
7a. Title in Foreign Language (in the case of translations)				
7b. Presented at (for conference papers) Title, place and date of conference				
8. Author 1 Surname, initials Broughton, L	9(a) Author 2 Beale, M I J	9(b) Authors 3,4... Deshmukh, V G I	10. Date	pp. ref.
11. Contract Number	12. Period	13. Project	14. Other Reference	
15. Distribution statement Unlimited				
Descriptors (or keywords) continue on separate piece of paper				
<p>Abstract We present the conclusions of the RSRE programme on the application of focused ion beams in microelectronics and review the literature published in this field. We discuss the design and performance of focused beam implanters and the viability of their application to semiconductor device fabrication. Applications in the areas of lithography, direct implantation and micromachining are discussed in detail. Comparisons are made between the use of focused ion beams and existing techniques for these fabrication processes with a strong emphasis placed on the relative throughputs. We present results on a novel spot size measurement technique and the effect of beam heating on resist. We also present the results of studies into implantation passivation of resist to oxygen plasma attack as basis for a dry development lithography scheme. A novel lithography system employing flood electron exposure from a photocathode which is patterned by a focused ion beam which can also be used to repair mask defects.</p>				

END

DATE
FILMED

2-87